RESEARCH ARTICLE SUMMARY

IMMUNOLOGY

Prenatal maternal infection promotes tissue-specific immunity and inflammation in offspring

Ai Ing Lim, Taryn McFadden, Verena M. Link, Seong-Ji Han, Rose-Marie Karlsson, Apollo Stacy, Taylor K. Farley, Djalma S. Lima-Junior, Oliver J. Harrison, Jigar V. Desai, Michail S. Lionakis, Han-Yu Shih, Heather A. Cameron, Yasmine Belkaid*

INTRODUCTION: One fundamental property of the immune system is its ability to develop memory of previous encounters, resulting in enhanced responsiveness to subsequent challenges. This phenomenon includes not only the adaptive immune system but also innate cells and tissue stem cells. The concept of host imprinting by infection leading to altered responses to subsequent challenge is of particular interest in the context of pregnancy, which represents a fundamental developmental window for the immune system.

RATIONALE: Most infections encountered by mammals, including those experienced during pregnancy, are mild and transient. How these infections shape offspring tissue immunity and tissue predisposition to inflammatory disorders in the long term remains to be addressed.

RESULTS: Infection of timed-pregnant dams (day 10.5) with an attenuated strain of the food-borne pathogen *Yersinia pseudotuberculosis* (*yopM*) was transient and maternally restricted. Adult offspring of previously infected dams harbored a higher number of T helper 17 (T_H17) cells but no other cell subsets in the small and large intestinal lamina propria. No changes were observed at other barrier tissues. Transfer of transgenic T cells specific for a commensal antigen revealed that maternal infection affected the offspring intestinal milieu in a manner that enhanced T_H17 cell reactivity toward the microbiota. Cross-fostering experiments demonstrated that the increased T_H17 cells resulting from maternal infection was imprinted in utero. Among various inflammatory mediators, the cytokine interleukin-6 (IL-6) was significantly increased in the serum of dams infected with *yopM*. Injection of IL-6 alone to pregnant dams significantly increased T_H17 cell numbers within the guts of offspring. Conversely, blockade of IL-6 in infected dams prevented this increase in offspring. Furthermore, injection of IL-6 to germ-free pregnant dams and conventionalization of their offspring after weaning revealed that prenatal establishment and postnatal maintenance of IL-6–mediated tissue imprinting are independent of the maternal microbiota but allow the offspring to mount enhanced T_H17 cell responses to postnatal microbiota exposure.

IL6RA was expressed in all fetal intestinal epithelial cells, and specific deletion of IL6RA from epithelial cells significantly reduced Th17 responses within the gut of offspring from IL-6–exposed dams. Using complementary approaches, including assay for transposase-accessible chromatin with high-throughput sequencing (ATAC-seq) and single-cell RNA sequencing, we found that increased IL-6 during pregnancy had immediate effects (on fetal cells) and long-term effects (in the adult offspring) on epithelial stem cell chromatin accessibility and downstream epithelial cell function, particularly increased expression of genes encoding for antigen presentation machinery and antimicrobial peptides.

Altered epithelial activation status suggested the possibility that this phenomenon may be associated with enhanced antimicrobial defense. To address this, we used an acute model of oral infection with *Salmonella* Typhimurium. Offspring from dams previously infected with *yopM* or injected with IL-6 during pregnancy developed enhanced resistance to *Salmonella* oral infection and dissemination. No differences were observed in controlling cutaneous *Candida albicans* infection, further supporting the idea that maternal imprinting of offspring is restricted to the gut compartment. However, enhanced exposure to IL-6 during pregnancy was associated with enhanced gut pathology in the context of naïve T cell transfer and dextran sulfate sodium–mediated colitis.

CONCLUSION: Our work proposes that a transient, mild infection encountered during prenatal development can impose lasting alterations to gut epithelial stem cells, resulting in an altered threshold of activation and enhanced resistance to gut infection. The impact of maternal infection was tissue specific and predominantly mediated by a single cytokine, IL-6, acting on epithelial stem cells during fetal development. Although this phenomenon can be coopted by the fetus to develop optimal immune fitness, altered offspring immunity imposed by maternal infection comes at the cost of enhanced susceptibility to mucosal inflammation. ■

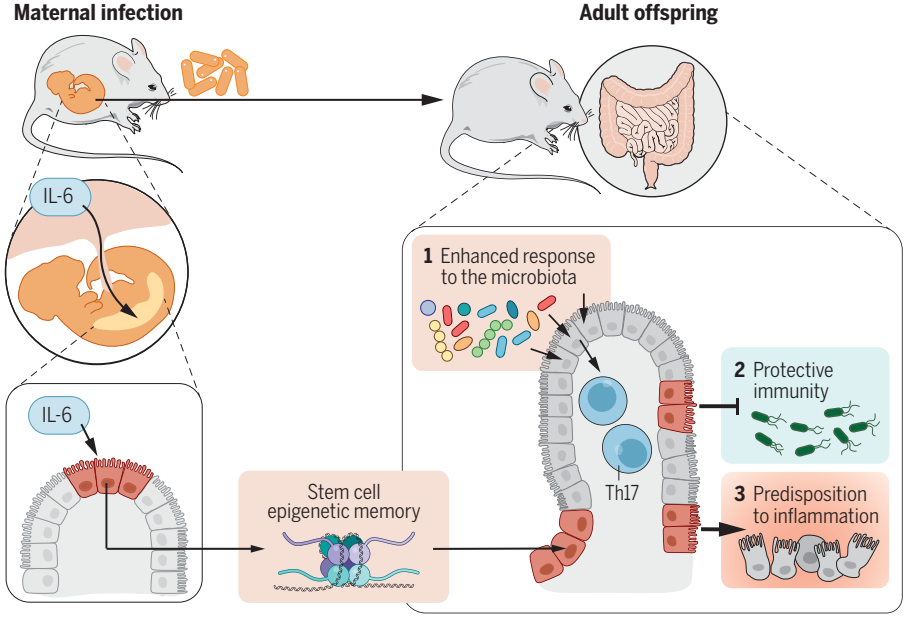

Maternal infection promotes offspring intestine-specific immunity and inflammation. The direct response of fetal intestinal epithelial cells to IL-6 during maternal infection confers an enduring epigenetic memory to adult intestinal epithelial stem cells. As such, offspring epithelial cells exhibit enhanced reactivity toward the microbiota and heightened ability to control oral infection. However, these responses come at the cost of greater predisposition to gut inflammation.

The list of author affiliations is available in the full article online.
*Corresponding author. Email: ybelkaid@niaid.nih.gov
Cite this article as A. I. Lim *et al.*, *Science* **373**, eabf3002 (2021). DOI: 10.1126/science.abf3002

READ THE FULL ARTICLE AT
https://doi.org/10.1126/science.abf3002

RESEARCH ARTICLE

IMMUNOLOGY

Prenatal maternal infection promotes tissue-specific immunity and inflammation in offspring

Ai Ing Lim[1], Taryn McFadden[1], Verena M. Link[1], Seong-Ji Han[1], Rose-Marie Karlsson[2], Apollo Stacy[1,3], Taylor K. Farley[1,4], Djalma S. Lima-Junior[1], Oliver J. Harrison[1]†, Jigar V. Desai[5], Michail S. Lionakis[5], Han-Yu Shih[6], Heather A. Cameron[2], Yasmine Belkaid[1,7]*

The immune system has evolved in the face of microbial exposure. How maternal infection experienced at distinct developmental stages shapes the offspring immune system remains poorly understood. Here, we show that during pregnancy, maternally restricted infection can have permanent and tissue-specific impacts on offspring immunity. Mechanistically, maternal interleukin-6 produced in response to infection can directly impose epigenetic changes on fetal intestinal epithelial stem cells, leading to long-lasting impacts on intestinal immune homeostasis. As a result, offspring of previously infected dams develop enhanced protective immunity to gut infection and increased inflammation in the context of colitis. Thus, maternal infection can be coopted by the fetus to promote long-term, tissue-specific fitness, a phenomenon that may come at the cost of predisposition to inflammatory disorders.

One fundamental property of the immune system is its ability to develop memory of previous encounters, resulting in enhanced responsiveness to subsequent challenges. Although immunological memory was initially characterized as a defining property of the adaptive immune system, a growing body of evidence supports the idea that components of the innate system can also be profoundly affected by inflammatory or infectious encounters, a phenomenon referred to as trained immunity (*1*). Tissue stem cells can also develop memory of previous insults, resulting in accelerated responses to subsequent challenges (*2*, *3*). Innate imprinting is usually transient, lasting a few weeks to months after exposure. However, parental experiences can be transferred across generations in invertebrates, a phenomenon that is also hypothesized to exist in vertebrates (*4*–*6*). Education of innate or stem cells by previous inflammatory insults has been associated with epigenetic reprograming (*2*, *3*, *7*), although the mechanisms underlying this fundamental property remain largely elusive and represent an active area of investigation. This revised understanding of immunity as a phenomenon encompassing the experiences of the whole organism as opposed to specialized cells provides a framework with which to understand the enhanced immune fitness observed in animals raised in physiological environments, in contrast to animals raised under highly controlled, laboratory settings (*8*, *9*).

The concept of host immune imprinting is of particular interest in the context of pregnancy, which represents a fundamental developmental window for the immune system. Pregnancy is associated with specific maternal adaptations that serve to maintain tolerance to the fetus (*10*). At the same time, the mother can contribute to offspring protection against pathogens through the transfer of immunomodulatory factors, including maternal antibodies and immune cells, in utero and through breastfeeding (*11*–*13*). Maternal immune activation has also been associated with altered offspring systemic T cell responses (*14*). However, how infection experienced by the mother during pregnancy shapes offspring tissue immunity in the long term remains poorly understood. Indeed, most of our current understanding derives from studies illustrating detrimental outcomes of severe maternal inflammation or infections with pathogens that are able to cross the placental barrier (*15*). How defined stressors encountered during pregnancy alter offspring predisposition to inflammatory disorders remains unclear. Mammals and their immune systems evolved in the face of a microbially rich environment, and frequent exposure to pathogens and associated protective immunity represents the norm rather than the exception. Host survival also requires prioritization of defense strategies that protect the host from tissue damage, in some cases by limiting infection severity without affecting the pathogen load, a phenomenon referred to as disease tolerance (*16*, *17*). As a result, by far most microbial encounters are expected to be associated with mild or no symptoms.

Here, we explored the possibility that maternal infection experienced during pregnancy could affect the offspring immune system in the long term. On the basis of the fundamental developmental processes that occur in utero, we proposed that specific signals experienced at specific developmental windows may imprint the fetus in a discrete and tissue-specific manner.

Maternally restricted infection induces tissue-specific alterations to offspring immunity

To assess the impact of maternally restricted infection on offspring immunity, we used an attenuated strain of the food-borne pathogen *Yersinia pseudotuberculosis*. This specific strain, which harbors a mutation in an effector protein (YopM) translocated by the type III secretion system, causes a mild and transient infection (*18*, *19*). Timed-pregnant dams were orally infected with the mutant strain (*yopM*) at gestation day 10.5 (Fig. 1A). This specific time point represents a critical developmental stage for the fetal immune system, characterized by the emergence of hematopoietic stem cells and the initiation of hematopoiesis (*20*, *21*). After *yopM* infection, dams experienced transient weight loss from days 5 to 8 after infection, but no other symptoms were observed (fig. S1A). Timed-pregnant dams transiently shed *yopM* in their stool (fig. S1B), and only 20% of pregnant females experienced transient bacterial dissemination to the liver and spleen (fig. S1C). In a manner comparable to nonpregnant mice (*18*), *yopM* was controlled in the intestines by day 5 after infection and cleared by day 9 (fig. S1B). No bacteria were detected in the fetal intestine (fig. S1B), placenta, or fetal liver (fig. S1C), as assessed by culture and polymerase chain reaction (PCR), at any time point tested. Moreover, infection did not affect litter sizes (fig. S1D). Thus, *yopM* infection represents a model of mild, maternally restricted infection.

We next compared the lymphocyte compartments of the adult offspring delivered by naïve versus previously infected dams. To this end, we characterized the number, frequency, and phenotype of T cells and innate lymphoid cells (ILCs) at barrier tissues, including the skin, the lung, and the small (siLP) and large intestinal lamina propria (liLP) of 5- to 8-week-old offspring (fig. S1E). Maternal infection during

[1]Metaorganism Immunity Section, Laboratory of Immune System Biology and Laboratory of Host Immunity and Microbiome, National Institute of Allergy and Infectious Diseases, National Institutes of Health, Bethesda, MD 20892, USA. [2]Section on Neuroplasticity, Mood and Anxiety Disorders Program, National Institute of Mental Health, National Institutes of Health, Bethesda, MD 20892, USA. [3]Postdoctoral Research Associate Training Program, National Institute of General Medical Sciences, Bethesda, MD 20892, USA. [4]Kennedy Institute of Rheumatology, Nuffield Department of Orthopaedics, Rheumatology and Musculoskeletal Sciences, University of Oxford, Oxford OX3 7FY, UK. [5]Fungal Pathogenesis Section, Laboratory of Clinical Immunology and Microbiology, National Institute of Allergy and Infectious Diseases, National Institutes of Health, Bethesda, MD 20892, USA. [6]Neuro-Immune Regulome Unit, National Eye Institute, National Institutes of Health, Bethesda, MD 20892, USA. [7]NIAID Microbiome Program, National Institute of Allergy and Infectious Diseases, National Institutes of Health, Bethesda, MD 20892, USA.
*Corresponding author. Email: ybelkaid@niaid.nih.gov
†Present address: Center for Fundamental Immunology, Benaroya Research Institute, Seattle, WA 98101, USA.

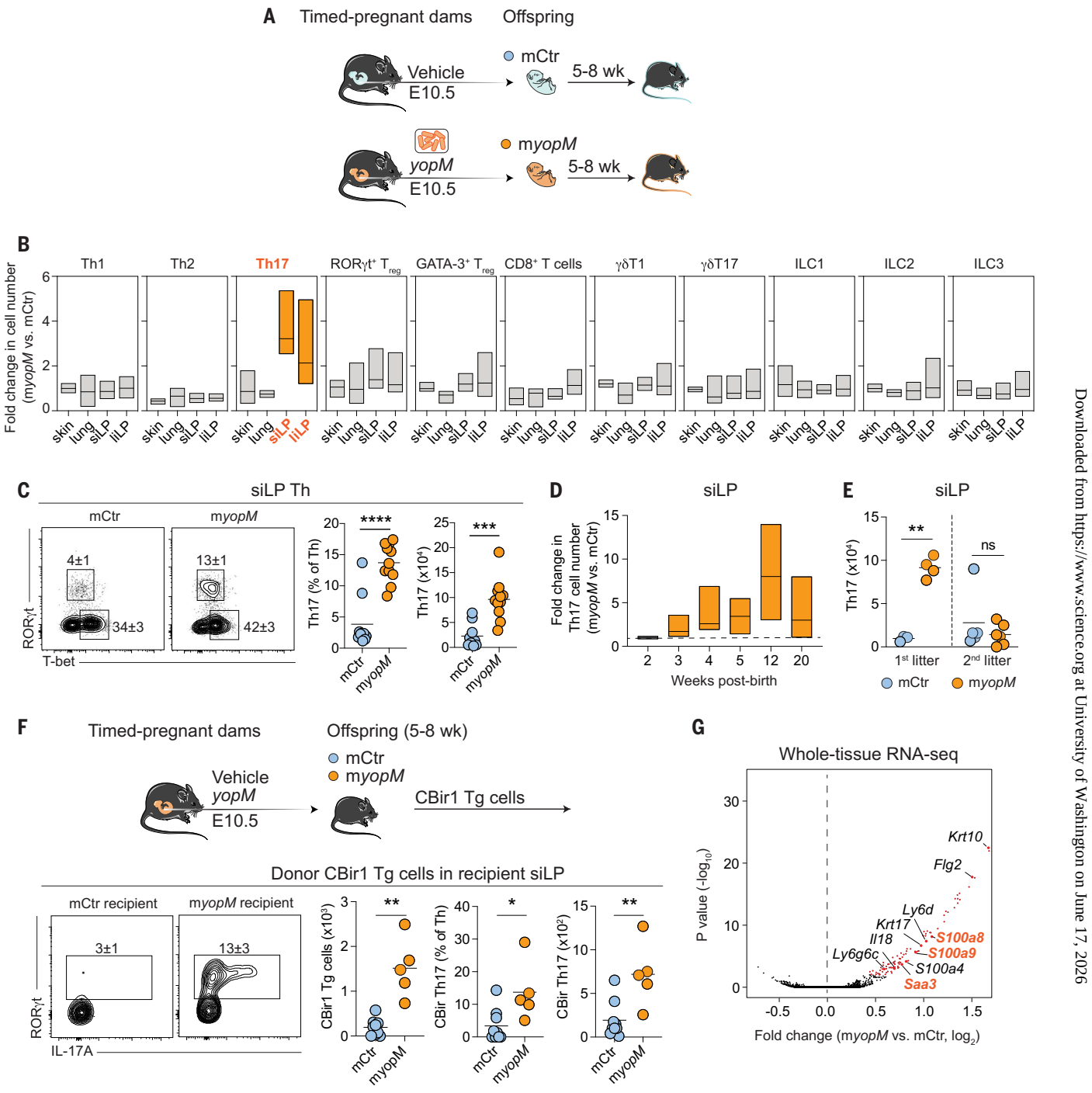

Fig. 1. Maternally restricted infection induces tissue-specific alterations to offspring immunity. (**A**) Timed-pregnant dams were orally administered vehicle (PBS) or *Y. pseudotuberculosis yopM* on gestation day 10.5 (E10.5), and their offspring, mCtr or m*yopM*, were analyzed at 5 to 8 weeks of age. (**B**) Fold change in cell number of lymphocyte subsets in ear skin, lung, siLP, and liLP of m*yopM* offspring compared with the mean of mCtr offspring. Cells were gated according to the schematic provided in fig. S1E. (**C**) Left: Representative contour plots of transcription factors expressed by offspring siLP T_H subsets (gated on live $CD45^+CD90.2^+TCR\beta^+CD4^+Foxp3^-$). Right: Frequency of T_H17 ($ROR\gamma t^+$) cells among total T_H cells, and total siLP T_H17 cell number. (**D**) Fold change in T_H17 cell number in the siLP of m*yopM* offspring compared with the mean of mCtr offspring at corresponding ages. (**E**) Total siLP T_H17 cell number in the offspring of vehicle-treated dams or dams infected during pregnancy (1st) or the offspring from a subsequent pregnancy of the same dams (2nd). (**F**) Donor CBir1 Tg cells (CD45.1) were transferred to congenic mCtr or m*yopM* offspring (CD45.2). Donor cells in the siLP of recipient offspring were analyzed for transcription factor expression and cytokine production after restimulation at days 10 to 12 after transfer. Contour plots were gated on live $CD45.1^+CD90.2^+TCR\beta^+CD4^+Foxp3^-$. (**G**) Whole-tissue RNA-seq of ileum from m*yopM* offspring compared with mCtr offspring. Up-regulated genes are denoted in red. (A to G) Data are representative of three independent experiments, each experiment with one or two pregnant dams per group using three to five offspring per pregnancy. Each dot represents an individual mouse. Numbers in representative flow plots indicate mean ± SD. $^*P < 0.05$; $^{**}P < 0.01$; $^{***}P < 0.001$; $^{****}P < 0.0001$; ns, not significant (two-tailed unpaired Student's *t* test). See also fig. S1.

pregnancy was associated with a significant and selective increase in the number and frequency of RORγt-expressing $CD4^+$ T (T_H17) cells in the siLP of offspring compared with animals delivered from naïve dams (Fig. 1, B and C). The increase in T_H17 cell number was restricted to the gut compartment and was not detected at other assessed barrier sites (Fig. 1B). Furthermore, no differences were observed in the number of other lymphocyte subsets, including T-bet–expressing $CD4^+$ T (T_H1) cells, GATA3-expressing $CD4^+$ T (T_H2) cells, Foxp3-expressing $CD4^+$ regulatory T cells [RORgt$^+$ regulatory T cell (T_{reg}) and $GATA3^+$ T_{reg}], $CD8^+$ T cells, γδ T cells (γδT1 and γδT17), and ILCs (ILC1, ILC2, and ILC3) in all the compartments assessed (Fig. 1B and fig. S1F). Increased accumulation of T_H17 cells within the siLP was detectable after weaning (at 3 weeks) and persisted throughout adulthood (up to 20 weeks) (Fig. 1D and fig. S1G). The impact of infection on the offspring gut immune system was not observed in subsequent litters from the same dams, supporting the idea that the ability of the dams to enhance offspring immunity was not caused by long-term maternal imprinting (Fig. 1E). Thus, a transient infection during pregnancy can impose long-lasting, tissue-specific alterations to offspring immunity.

We next assessed whether this phenomenon was T cell intrinsic or caused by an altered tissue environment. To this end, we evaluated the ability of the offspring delivered by control or previously infected dams to mount de novo responses to the microbiota. Transgenic T cells specific for a defined commensal-derived antigen (CBir1 Tg cells) (*22*) were transferred into the offspring of naïve or previously infected dams (Fig. 1F). Consistent with previous studies (*22*, *23*), a small number of CBir1 Tg cells accumulated in the siLP of control mice, where they remained largely undifferentiated (Fig. 1F). By contrast, a higher number of CBir1 Tg cells accumulated in the siLP of offspring delivered by previously infected dams, with a significant fraction of those differentiated toward a T_H17 cell phenotype (Fig. 1F). Thus, maternal infection can affect the offspring intestinal milieu in a way that enhances reactivity toward the microbiota and promotes T_H17 cell responses. In support of this observation, whole-tissue RNA sequencing of the small intestine revealed the up-regulation of genes encoding for factors known to promote local licensing of T_H17 cells (serum amyloid A, *Saa3*) (*24*) and of genes downstream of T_H17 cell responses (*S100a8*, and *S100a9*) (Fig. 1G).

Maternally restricted infection alters offspring intestinal immunity in utero independently of the microbiota

Infection can affect the composition, localization, and function of the microbiota (*25*–*27*). As such, we next explored the possibility that enhanced T_H17 cell responses could be associated with acquisition of infection-altered maternal microbiota. The microbiota of the offspring delivered by infected and naïve dams clustered closely to each other, as demonstrated by Bray–Curtis principal coordinates analysis (Fig. 2, A and B). Although no significant shifts occurred at the phylum level (Fig. 2C), a small number of taxa belonging to *Bacteroidales* and *Coriobacteriales* were increased, whereas a few taxa belonging to the *Clostridiales* and *Erysipelotrichales* were decreased, in the offspring of previously infected dams (Fig. 2D). To assess the potential contribution of the altered microbiota to offspring immunity, newborns delivered by control and previously infected dams were cross-fostered until weaning (Fig. 2E). Offspring delivered by previously infected dams and fostered by control dams harbored a number of siLP T_H17 cells comparable to those of offspring delivered and fostered by previously infected dams (Fig. 2, F to I). Conversely, offspring delivered by control dams and fostered by previously infected dams did not have an increased number of T_H17 cells within the siLP (Fig. 2, F to I). These data support the hypothesis that the heightened intestinal T_H17 cell responses caused by maternal infection were acquired in utero and did not result from the transfer of altered maternal microbiota after birth or during lactation.

Increasing maternal IL-6 levels during pregnancy is sufficient to enhance intestinal T_H17 cell responses and reactivity to the microbiota in offspring

Soluble factors, including cytokines, can cross the placental barrier (*28*, *29*). To assess a potential role for maternal soluble factors, we transferred sera from infected dams to naïve dams at gestation days 13.5 and 15.5 (Fig. 3A). We confirmed that no bacteria were transferred and that the recipient dams did not mount an immune response against *yopM* (fig. S2, A and B). Injection of sera from previously infected dams was sufficient to increase the offspring intestinal T_H17 cell number in a manner comparable to that observed after maternal *yopM* infection (Fig. 3A). Assessment of cytokine and chemokine levels in the sera of *yopM*-infected pregnant dams at different time points after infection revealed that four cytokines were significantly enriched: interleukin-6 (IL-6), interferon-γ (IFN-γ), granulocyte colony-stimulating factor (G-CSF), and tumor necrosis factor-α (TNF-α) (Fig. 3B). A single injection of IL-6, but not IFN-γ, G-CSF, or TNF-α, to naïve pregnant dams was sufficient to increase the number of T_H17 cells in the siLP of offspring (fig. S2C) in a dose-dependent manner (Fig. 3C). After injection, dams had circulating IL-6 levels that were comparable to those previously reported in the context of various infection models (*30*, *31*) and returned to baseline by day 3 after injection. Furthermore, IL-6 was not increased in the milk. In support of potential transplacental transfer, IL-6 levels were increased in fetal sera after both maternal *yopM* infection and IL-6 injection (fig. S2D).

IL-6 has been previously linked to various biological outcomes in the context of pregnancy, including gestational disorders (*32*). Furthermore, a previous study showed that IL-6 enhanced IL-17A production in dams, the production of which can contribute to the development of an autism-like disorder in offspring (*33*). However, in our present study, the enhanced IL-6 levels during pregnancy had no adverse impact on pregnancy and were not associated with detectable impairment in social preference of adult offspring (fig. S2E). One notable difference in experimental settings was that our study was conducted in mice devoid of segmented filamentous bacteria (SFB), a group of bacteria previously implicated in altered behaviors in progeny (*34*).

As observed in the context of maternal infection, IL-6 injection significantly increased the number of T_H17 cells in all sections of the offspring small intestine (Fig. 3D). IL-6 injection was also associated with a significant increase in the level of IL-17A production by T_H17 cells in the jejunum and the ileum (Fig. 3, E and F). Supporting enhanced tissue licensing of IL-17A signaling (*24*), both maternal infection and IL-6 injection enhanced serum amyloid A production in the jejunum and the ileum (Fig. 3G). IL-6 injection also induced a small increase in the number of $CD8^+$ T cells in the duodenum (fig. S3A). Droplet-based 3′ single-cell RNA sequencing (scRNA-seq) analysis revealed that siLP T_H17 cells of offspring from IL-6–injected dams expressed higher levels of canonical T_H17 cell markers (*Maf*, *Ahr*, *Ccr6*, *Il17a*, *Il17f*, and *Il22*) but not of genes associated with pathogenic T_H17 cells (*35*, *36*), including *Tbx21*, *Gmzb*, *Ifng*, and *Csf2* (Fig. 3, H and I). Thus, in agreement with the concept that maternal infection enhances T_H17 cell responses to the microbiota (Fig. 1F), T_H17 cells that accumulate under these conditions are nonpathogenic and likely involved in the control of barrier function. Indeed, we could not detect any differences in the distance between gut bacteria and host epithelium in offspring from IL-6–treated or infected dams (fig. S3, B and C). To address the possibility that IL-6 is not only sufficient but also necessary for the impact of maternal *yopM* infection on offspring immunity, pregnant dams were treated with a neutralizing IL-6 antibody before *yopM* infection (Fig. 3J). This treatment did not affect the ability of the pregnant dams to control the infection (fig. S3D). IL-6 neutralization during maternal infection significantly reduced the accumulation of T_H17 cells in the siLP of offspring (Fig. 3J). Collectively, our findings support the

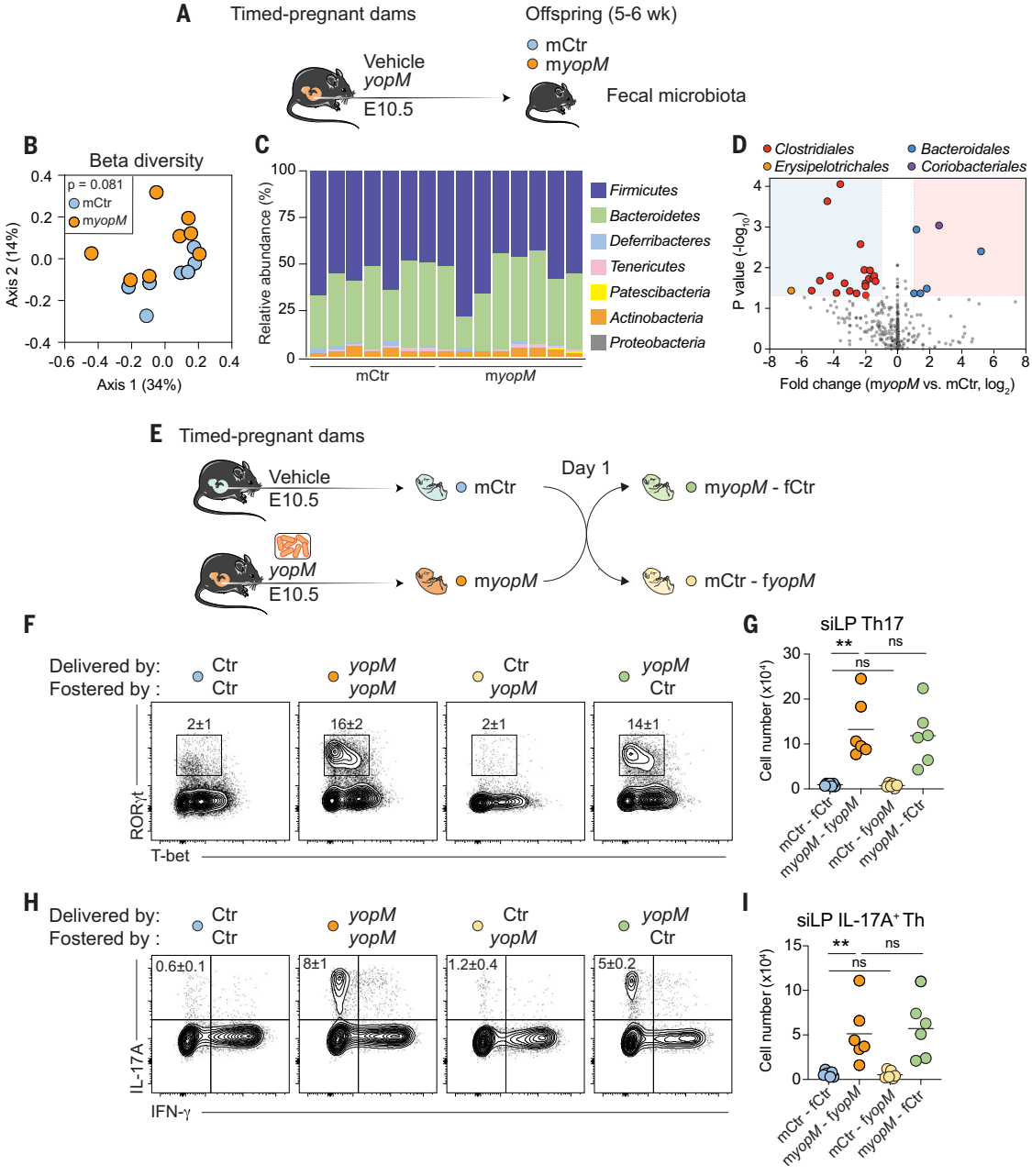

Fig. 2. Maternally restricted infection alters offspring intestinal immunity in utero independently of the microbiota. (**A**) Timed-pregnant dams were orally administered vehicle (PBS) or *yopM*, and fecal microbiota from their offspring, mCtr or m*yopM*, were profiled at 5 to 6 weeks of age by 16*S* rRNA gene sequencing. (**B**) Principal coordinates analysis plot displaying the Bray–Curtis distances between the fecal 16*S* profiles of mCtr and m*yopM* offspring. Percentages represent the variance corresponding to each principal coordinate. Significance was determined by PERMANOVA. (**C**) Relative abundance of phyla in the mCtr and m*yopM* fecal microbiota. (**D**) Volcano plot of fecal microbiota species (sequence variants). The taxonomic families of significantly altered species are indicated. (**E**) Cross-fostering experiment. Within 24 hours after birth, offspring delivered by vehicle-treated dams were transferred to previously infected dams (mCtr-f*yopM*) or vice versa (m*yopM*-fCtr). Offspring were cross-fostered until weaning and analyzed at 5 to 8 weeks of age. In the control groups, the offspring were raised by their own dams (mCtr-fCtr, m*yopM*-f*yopM*). (**F**) Representative contour plots of transcription factors expression by T_H cell subsets in the offspring siLP. (**G**) Total siLP T_H17 (RORγt^+) cell number. (**H**) Representative contour plots of cytokine production by T_H cells after restimulation. (**I**) Total cell number of siLP IL-17A–producing T_H cells. In (A) to (I), all flow plots were gated on live $CD45^+CD90.2^+TCR\beta^+CD4^+Foxp3^-$. Numbers in representative flow plots indicate mean ± SD. Data are representative of three independent experiments, each experiment with one pregnant dam per group using three to six offspring per pregnancy. Each dot represents an individual mouse. $^{**}P < 0.01$; ns, not significant (one-way ANOVA multiple-comparisons test).

idea that increased levels of maternal IL-6, elicited by transient infection during pregnancy, alter offspring intestinal immunity.

Although a shift in the maternally acquired microbiota was not responsible for altered offspring immunity (Fig. 2, D and G), we assessed whether the maternal microbiota was required during pregnancy and/or after delivery for the remodeling of the offspring immune response. To address this point, germ-free pregnant dams were injected with IL-6 or vehicle control. IL-6 injection did not cause enhanced T_H17 cell accumulation in the offspring siLP if the offspring were maintained under germ-free conditions (Fig. 3K). However, reintroduction of the microbiota (conventionalization) after weaning was associated with enhanced T_H17 cell number in the offspring from IL-6–injected dams but not in those from control dams (Fig. 3K). Thus, prenatal establishment and postnatal maintenance of IL-6–mediated tissue imprinting is independent of the maternal microbiota but allows the offspring to mount enhanced T_H17 cell responses in response to postnatal exposure to the microbiota.

Increasing maternal IL-6 levels during pregnancy alters the epigenome of fetal IECs

Responses to IL-6 signaling are mediated by the IL-6 receptor (IL6RA, also known as CD126),

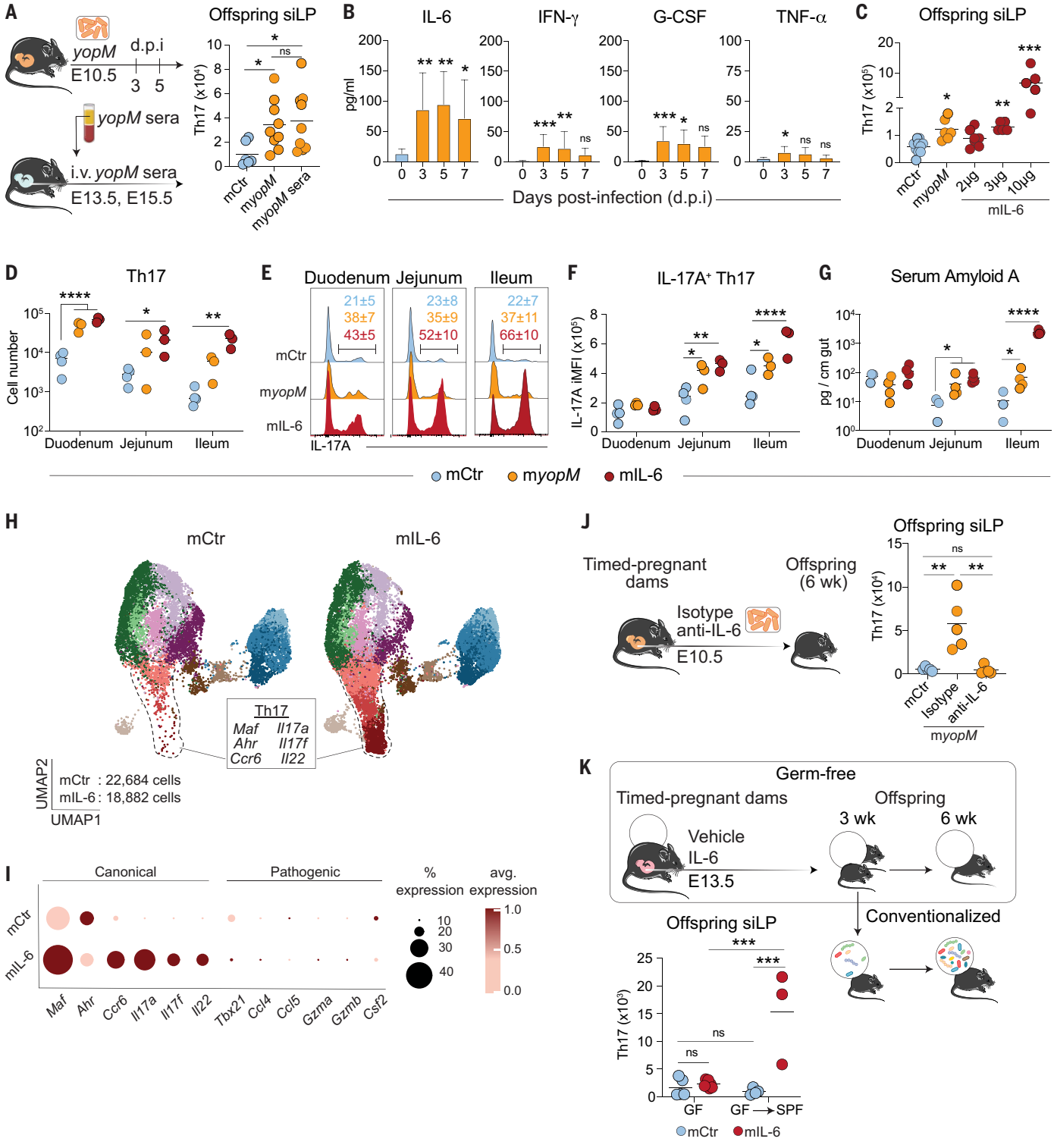

Fig. 3. Increasing maternal IL-6 levels during pregnancy is sufficient to enhance offspring intestinal T_H17 and responsiveness to the microbiota. (**A**) Left: Timed-pregnant dams were infected with *yopM*, and sera collected at 3 and 5 days postinfection (d.p.i.) were transferred intravenously to naïve pregnant dams at E13.5 and E15.5. Right: Total T_H17 cell number in the siLP of 6-week-old offspring. (**B**) Timed-pregnant dams were orally infected with *yopM* at E10.5. Sera collected before infection or at 3, 5, or 7 d.p.i. were assayed for cytokine and chemokine levels. (**C**) Timed-pregnant dams were orally administered vehicle or *yopM* or intravenously injected with the indicated doses of IL-6, and their offspring (mCtr, m*yopM*, or mIL-6) were analyzed at 6 weeks of age for total siLP T_H17 cell number. (**D** to **G**) siLP subcompartments from adult offspring delivered by mCtr, m*yopM*, or dams intravenously injected with 10 μg IL-6 (mIL-6) were analyzed for total T_H17 cell number (D), frequency of IL-17A–producing T_H17 cells (E), integrated mean fluorescence intensity (iMFI) of IL-17A production by T_H17 cells [iMFI = (IL-17A MFI) × (frequency of IL-17A–producing T_H17 cells)] (F), and serum amyloid A levels (G). (**H** and **I**) Total $CD4^+$ T cells were sorted from the siLP of mCtr or mIL-6 at 6 weeks of age and analyzed by scRNA-seq. (H) UMAP projection plots showing the expression

profiles of CD4$^+$ T cells. Colors represent cells clustered together on the basis of similarity of global gene expression. (I) Dot plot indicating level and abundance of expression of canonical or pathogenic gene signatures of the T_H17 cell cluster. (**J**) Left: *yopM*-infected dams were pretreated with 1 mg of anti-IL-6 monoclonal antibody or the isotype control 2 hours before infection. Right: Total T_H17 cell number in the siLP of 6-week-old offspring. (**K**) Top: Germ-free timed-pregnant dams were intravenously injected with vehicle or 10 μg of IL-6 at E13.5, and their offspring, mCtr or mIL-6, were maintained under germ-free conditions or conventionalized in a specific-pathogen-free facility from 3 to 6 weeks of age. Bottom: total T_H17 cell number in the siLP of 6-week-old offspring. In (A) to (K), data are representative of three independent experiments [(A) to (G) and (J) to (K)], each experiment with one or two pregnant dams per group using three to five offspring per pregnancy, or one experiment [(H) and (I)] with three pregnant dams per group using one offspring per pregnancy. Each dot represents an individual mouse. *P < 0.05; **P < 0.01; ***P < 0.001; ****P < 0.0001; ns, not significant [ANOVA multiple-comparisons test, one-way in (A) to (C) and (J) and two-way in (D) to (G) and (K)]. See also figs. S2 and S3.

the glycoprotein 130 complex, and the JAK-STAT3 pathway (*37*). IL-6 has also been shown to cross both human and murine placenta (*28*, *38*, *39*). To investigate the impact of IL-6 on the fetal intestine, we first assessed expression of IL6RA in fetal intestinal epithelial and hematopoietic cells. We found that IL6RA was expressed at an intermediate level in all fetal intestinal epithelial cells (IECs) (EpCAM$^+$) and at a high level in a fraction of hematopoietic cells (CD45$^+$) (Fig. 4, A and B). By contrast, IL6RA was not expressed by fetal lung epithelial cells (EpCAM$^+$) or fetal skin keratinocytes (CD49f$^+$) (Fig. 4C). Of relevance to human settings, reanalysis of a published dataset (*40*) revealed that *IL6R* is also expressed at intermediate levels by human fetal IECs (fig. S4A). To identify cellular compartments that can respond to IL-6, we evaluated STAT3 phosphorylation at days 1 and 3 after *yopM* infection or IL-6 injection. A small fraction of IECs expressed phosphorylated STAT3 (pSTAT3) at steady state, supporting the idea that the JAK-STAT3 pathway may already be constitutively engaged during epithelial cell development (Fig. 4D and fig. S4B). At day 3 after maternal infection or IL-6 injection, pSTAT3 levels were further increased in fetal IECs but not in hematopoietic cells (Fig. 4D).

To test the possibility that IECs may be the direct target tissue imprinted by maternal IL-6 during infection, we characterized the epigenetic and transcriptional landscape of fetal IECs from control and IL-6–injected dams using an assay for transposase-accessible chromatin with high-throughput sequencing (ATAC-seq) and RNA-seq (fig. S4C). Genes important for IEC identity (including *Epcam*, *Vil1*, *Cdx1*, and *Cdx2*) (*41*, *42*) were equally accessible in fetal IECs from control and IL-6–injected dams (fig. S4D). Open chromatin regions in fetal IECs were enriched in transcription factor binding motifs (fig. S4E) that were previously implicated in intestinal development (CDX1/2), IEC differentiation (GATA and HNF4G), and epithelial cell identity establishment (KLF) (*43*). However, on a genome-wide level, fetal IEC chromatin accessibility was substantially increased after injection of IL-6 during pregnancy, with 2118 regions more accessible in fetuses from IL-6–injected dams (greater than a twofold change), compared with only four regions in IECs from fetuses from control dams (Fig. 4E). The differentially accessible promoter regions revealed enrichment of genes associated with intestinal physiological functions, including peptide transport, stem cell division, epithelium development, and T_H cell differentiation (e.g., *Jak2* and *Il10rb*) (Fig. 4F). By contrast, transcriptomic analysis showed minor alterations in fetal IECs (fig. S4F). Thus, exposure to IL-6 during development increases global chromatin accessibility of fetal IECs with minor impacts on their transcriptional landscape.

To further assess the contribution of IL-6 signaling on the ability of fetal IECs to regulate intestinal immunity, we specifically deleted the IL-6 receptor gene *Il6ra* from IECs (Fig. 4G). To this end, we used a breeding scheme allowing IL-6 signaling to be intact in the dams (*Il6ra*$^{fl/fl}$ *Vil1*$^{Cre-}$) and for IECs of the offspring to be either *Il6ra* sufficient (*Il6ra*$^{fl/fl}$ *Vil1*$^{Cre-}$) or *Il6ra* deficient (*Il6ra*$^{fl/fl}$ *Vil1*$^{Cre+}$). Confocal imaging confirmed selective ablation of IL6RA in IECs in *Il6ra*$^{fl/fl}$ *Vil1*$^{Cre+}$ mice (fig. S5, A and B). After injection of IL-6 during pregnancy, intestinal T_H17 cells were significantly reduced in the gut of *Il6ra*$^{fl/fl}$ *Vil1*$^{Cre+}$ offspring compared with *Il6ra*$^{fl/fl}$ *Vil1*$^{Cre-}$ littermate controls (Fig. 4G). Thus, IL-6 signaling in fetal IECs is sufficient and necessary to confer long-term intestinal immune alterations.

Prebirth IL-6 exposure alters chromatin accessibility and transcriptome of intestinal epithelial stem cells

Prior lineage-tracing studies revealed that all fetal IECs can contribute to the adult intestinal epithelial stem cell (EpSC) pool that is characterized by *Lgr5* expression (*44*). To address the possibility that alterations in fetal IECs may have long-term consequences on adult EpSCs, we assessed the chromatin accessibility of EpSCs (EpCAM$^+$Lgr5$^+$) from 6-week-old offspring delivered by control or IL-6–injected dams using ATAC-seq (Fig. 5A and fig. S6A). Chromatin accessibility was increased in EpSCs of adult offspring delivered by IL-6–injected dams, with 1006 regions more open (greater than a twofold change), compared with only 71 regions in EpSCs of control offspring (Fig. 5B). As anticipated based on the profound changes in epithelial cells occurring after birth and during weaning (*45*, *46*), open chromatin sites were largely distinct from those observed in the fetuses, with only 17 common peaks (<1% of the fetus) shared between fetal IECs and adult EpSCs (fig. S6B). Differentially accessible promoters found in adult EpSCs of offspring from IL-6–injected dams showed enrichment of genes involved in MAPK activation, cytokine signaling, and defense responses (e.g., *Alox5ap*, *Ptgs2*, *Mgst2*, and *Ffar3*) (Fig. 5C).

In adults, intestinal EpSCs constantly self-renew and differentiate into diverse subsets of epithelial cells endowed with discrete functions (*47*). Thus, we used droplet-based 3′ scRNA-seq to evaluate the potential consequences of maternal IL-6–mediated EpSC alterations on the composition and transcriptome of IECs (Fig. 5D). We focused our analysis on the duodenum and ileum, where we observed the largest increase in T_H17 cells after maternal IL-6 injection (Fig. 3D). Unsupervised clustering partitioned the IECs isolated from offspring delivered by control (n = 3, 4929 cells) and IL-6–injected (n = 3, 4112 cells) dams into 21 clusters (Fig. 5E and fig. S7A). Each cluster was identified (fig. S7B) on the basis of signature genes associated with distinct cell types and differentiation states (*48*). No significant differences were observed in cell composition between offspring delivered by control and IL-6–injected dams (Fig. 5F). By contrast, IL-6 injection imposed discrete transcriptomic alterations in defined subsets of IECs, including stem cells, transit-amplifying cells, and subsets of enterocytes at various stages of differentiation (fig. S7C). Genes encoding canonical components of the major histocompatibility complex II (MHCII) machinery, including *Cd74*, *H2-Aa*, and *H2-Ab1*, were strongly enriched in both stem cells and enterocytes of offspring delivered by IL-6–injected dams compared with control dams, with the strongest differences observed in the duodenum (Fig. 5G and fig. S7C). The expression of MHCII and genes encoding for the antigen presentation machinery by EpSCs has recently been reported to be microbiota dependent and to contribute to epithelial cell differentiation (*49*, *50*). IL-6 injection during pregnancy was also associated with increased expression of genes encoding antimicrobial peptides (e.g., *Reg3b* and *Reg3g*) in enterocytes (Fig. 5G). Thus, an increase in IL-6 during pregnancy can have a long-lasting impact on EpSC chromatin accessibility and downstream epithelial cell function.

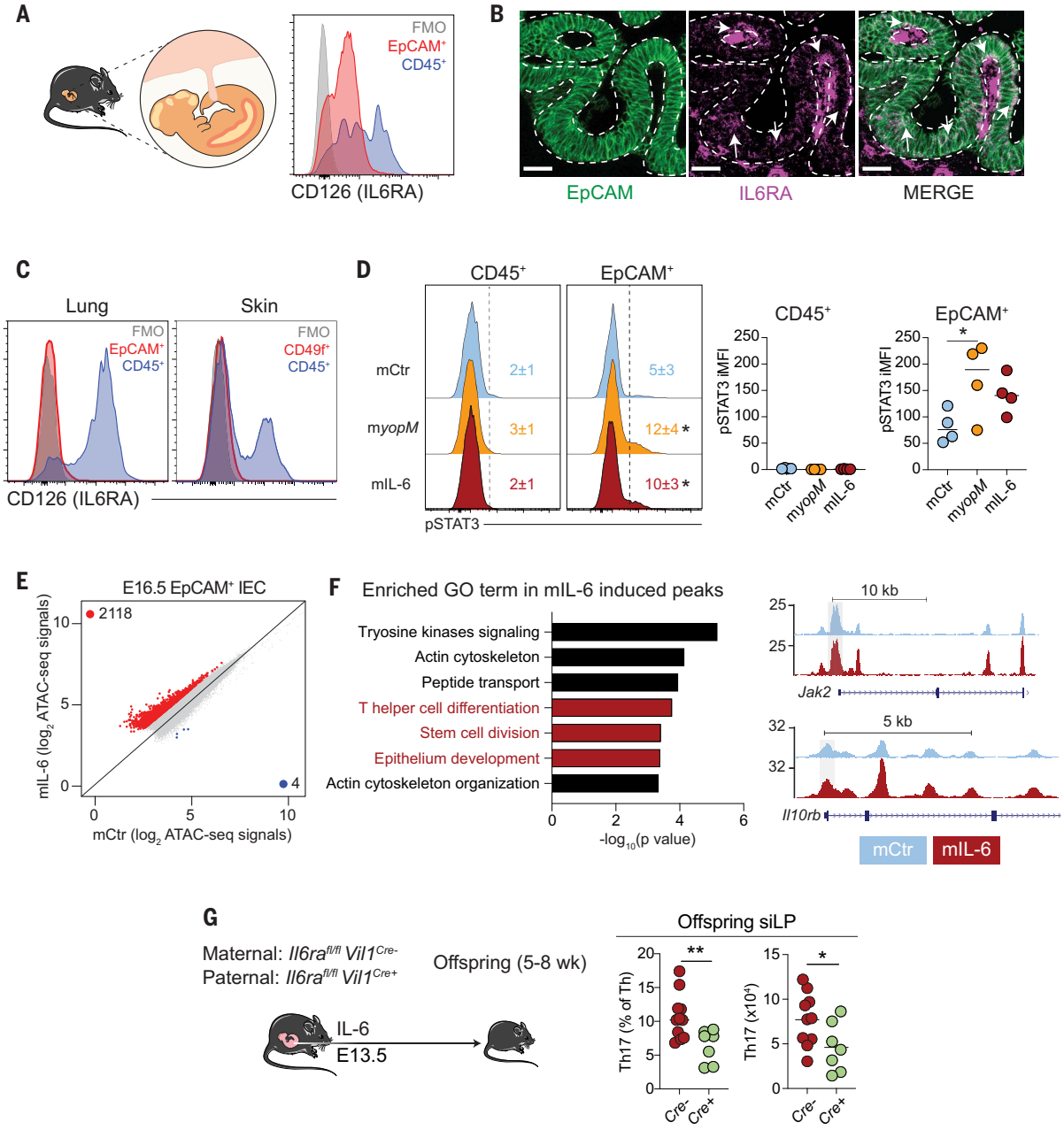

Fig. 4. Increasing maternal IL-6 levels during pregnancy alters the epigenome of fetal IECs. (**A**) Left: Fetal intestines were assessed for IL6RA (CD126) expression. Right: Representative histogram showing IL6RA expression by fetal IECs (IECs, $CD45^{-}EpCAM^{+}$) and hematopoietic cells ($CD45^{+}$) at E15.5. FMO, fluorescence minus one control. (**B**) Representative micrograph of fetal intestines stained for EpCAM and IL6RA at E15.5. Arrows point to IL6RA expressed by $EpCAM^{+}$ IECs (denoted by dashed line). Scale bars, 30 μm. (**C**) Representative histogram showing IL6RA expression by fetal lung epithelial cells ($CD45^{-}EpCAM^{+}$), fetal skin keratinocytes ($CD45^{-}CD49f^{+}$), and hematopoietic cells ($CD45^{+}$) at E15.5. (**D**) Left: Representative histogram of pSTAT3 expression by fetal hematopoietic cells or IECs from dams at 3 days after treatment with vehicle (mCtr), *yopM* (m*yopM*), or 10 μg IL-6 (mIL-6). Right: iMFI of pSTAT3 in hematopoietic cells ($CD45^{+}$) or IECs ($EpCAM^{+}$). (**E** and **F**) ATAC-seq data of fetal IECs from dams 3 days after treatment with vehicle (mCtr) or intravenous injection with 10 μg of IL-6 (mIL-6). (E) Scatter plot of all accessible chromatin regions. Red and blue dots correspond to regions that were differentially accessible by more than twofold in the IECs of mIL-6 fetuses and mCtr fetuses, respectively. (F) Left: Top Gene Ontology (GO) terms that were enriched in differentially accessible promoter regions (peaks within 3 kb of the next transcription start site, fold change >2) of mIL-6 fetuses compared with mCtr fetuses. Right: UCSC Genome Browser snapshots of genes of interest. Promoters open in mIL-6 offspring are highlighted in gray boxes. (**G**) *Il6ra* was deleted from IECs by crossing $Il6ra^{fl/fl}$ $Vil1^{Cre-}$ females to $Il6ra^{fl/fl}$ $Vil1^{Cre+}$ males. Dams were injected with 10 μg of IL-6, and offspring were analyzed at 5 to 8 weeks of age for siLP T_H17 cells. In (A) to (G), data are representative of three independent experiments [(A) to (D) and (G)], each experiment with one to three pregnant dams per group, or one experiment [(E) and (F)] with three pregnant dams per group using four to seven offspring per pregnancy. $^{*}P < 0.05$; $^{**}P < 0.01$ [two-tailed unpaired Student's *t* test in (G) and one-way ANOVA multiple-comparisons test in (D)]. See also figs. S4 and S5.

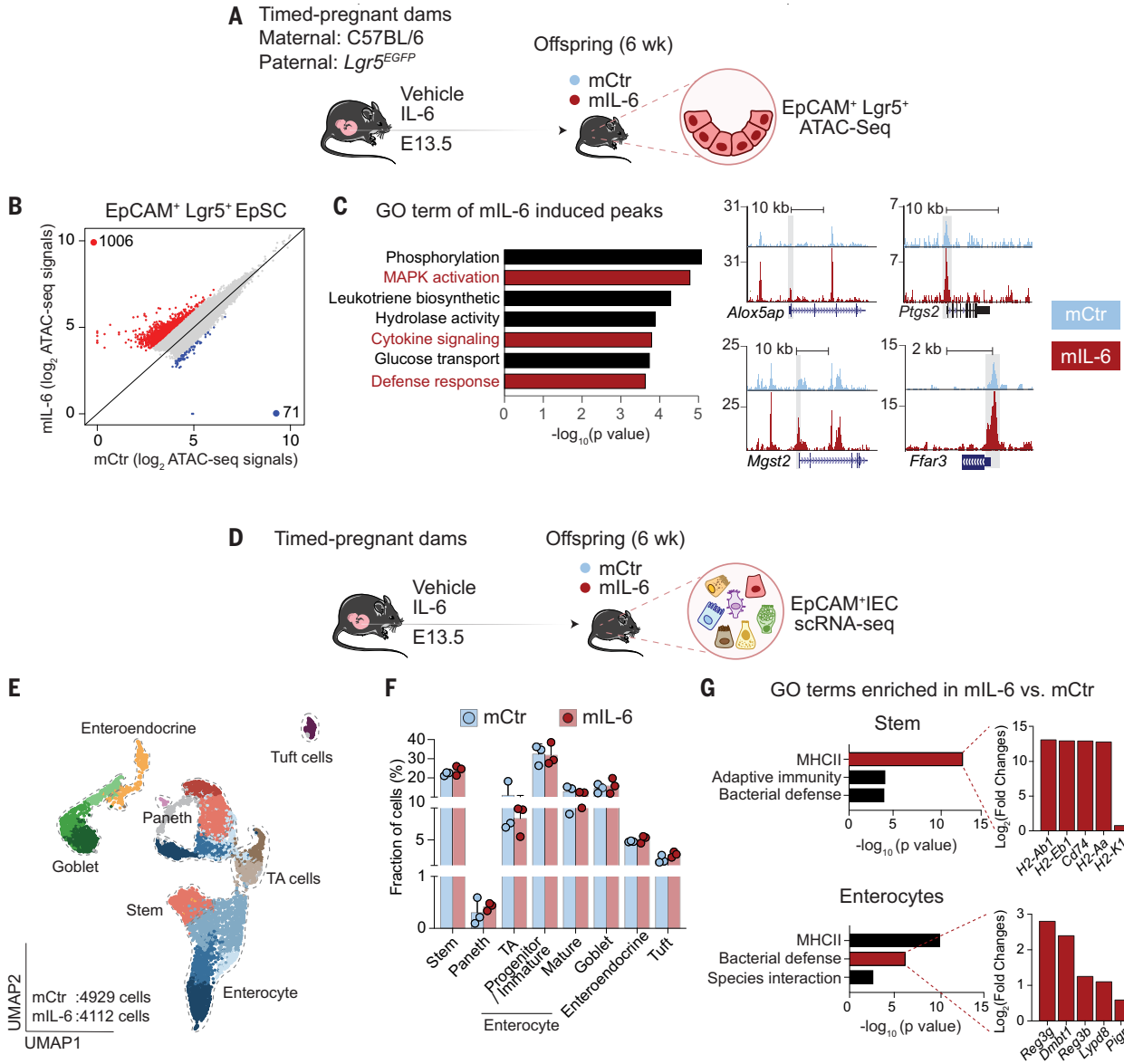

Fig. 5. Increasing maternal IL-6 levels during pregnancy alters the chromatin accessibility and transcriptome of offspring intestinal epithelial stem cells. (**A**) Timed-pregnant dams were injected with vehicle or 10 μg of IL-6 at E13.5. Intestinal EpSCs were sorted from their offspring, mCtr or mIL-6, for ATAC-seq at 6 weeks of age. (**B**) Scatter plot showing open chromatin regions. Red and blue dots correspond to regions that were differentially accessible by more than twofold in the EpSCs of mIL-6 and mCtr offspring, respectively. (**C**) Left: GO term analysis of differentially accessible promoter regions (peaks within 3 kb of the next transcription start site, fold change >2) in mIL-6 EpSC compared with mCtr EpSC. Right: UCSC Genome Browser snapshots of genes involved in cytokine signaling. Promoters open in mIL-6 offspring are highlighted in gray boxes. (**D**) IECs were sorted from mCtr or mIL-6 offspring for scRNA-seq at 6 weeks of age. (**E**) UMAP projection of IEC subsets, assigned on the basis of the 25 most differentially expressed genes in each subset versus all other cells. (**F**) Frequency of each IEC subset. (**G**) The top three GO terms that were enriched in stem cells and enterocytes of mIL-6 offspring. For selected GO terms highlighted in red, the top five genes up-regulated in mIL-6 offspring are shown. Data are from one experiment with three pregnant dams per group using one offspring per pregnancy. See also figs. S6 and S7.

Maternal infection or IL-6 exposure promotes offspring intestinal protective immunity and inflammation

Altered epithelial activation status and enhanced T cell responses to the microbiota in the gut of offspring of previously infected or IL-6–injected dams pointed to the possibility that this phenomenon may be associated with enhanced antimicrobial defense. To address this hypothesis, we used an acute model of oral infection with *Salmonella enterica* serovar Typhimurium (*S.* Typhimurium) (Fig. 6A). At the dose and route of infection used, *S.* Typhimurium primarily invades IECs before disseminating to distal organs and causing host lethality (*51*). Although no differences in bacterial shedding were observed at days 1 and 2 after infection, by day 4, offspring of IL-6–injected dams displayed a 1- to 2-log reduction in bacterial burden in their feces and Peyer's patches compared with the offspring of control dams (Fig. 6, B and C). Enhanced IL-6 during pregnancy also reduced bacterial dissemination to distal organs in offspring, with a 2- to 3-log decrease in bacterial burden in the mesenteric lymph nodes, liver, and spleen compared with controls (Fig. 6C) and significantly improved offspring survival rates after infection (Fig. 6D). Consistent with enhanced control of the infection, lipocalin-2, a marker

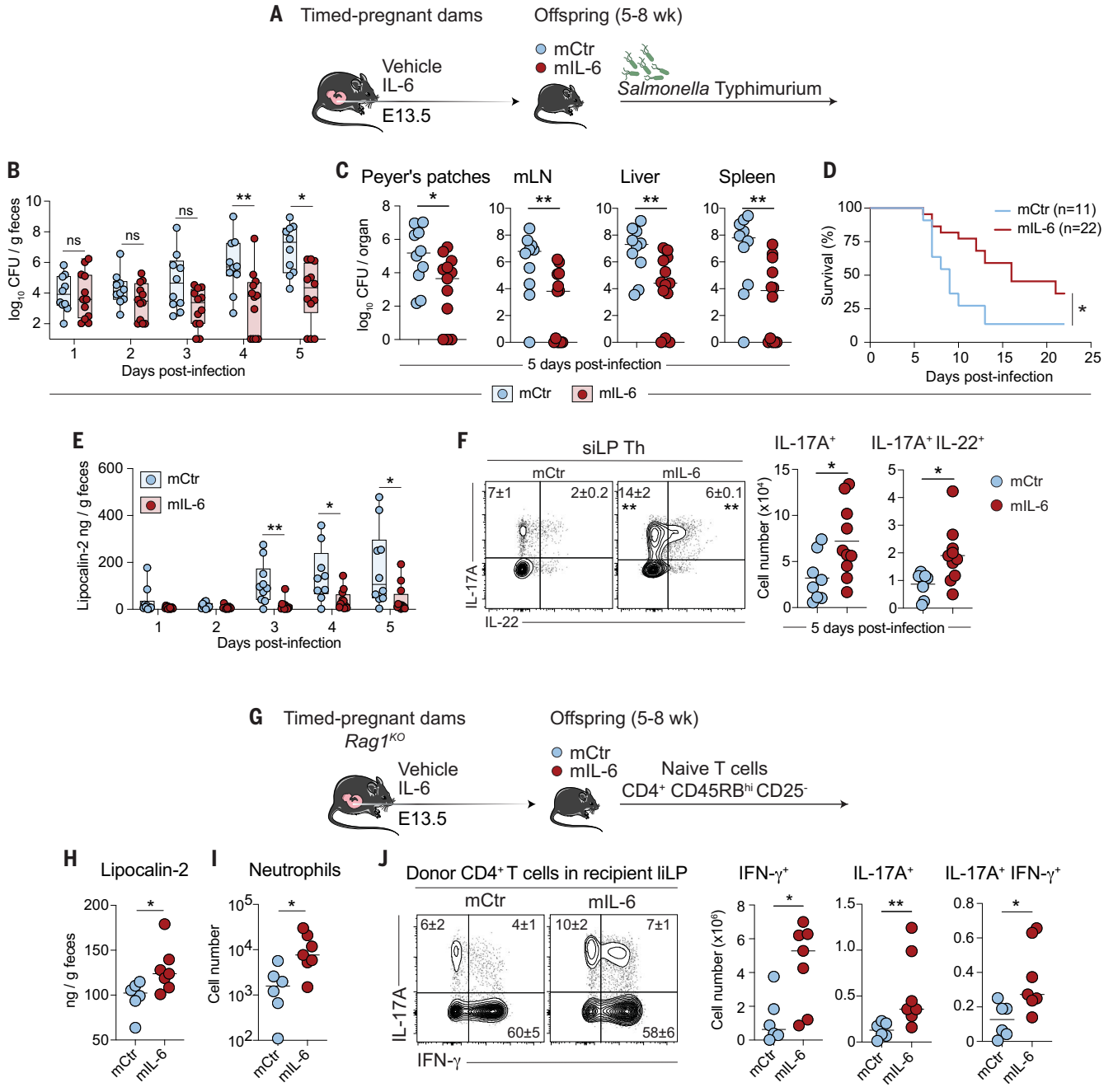

Fig. 6. Maternal infection or IL-6 exposure promotes offspring intestinal protective immunity and inflammation. (**A**) Timed-pregnant dams were injected with vehicle or 10 μg of IL-6 at E13.5, and their offspring (mCtr or mIL-6) were orally administered *S.* Typhimurium at 5 to 8 weeks of age. (**B** and **C**) *S.* Typhimurium burden in feces at days 1 to 5 after infection (B) and in tissues at day 5 after infection (C). (**D**) Survival curve. (**E**) Fecal lipocalin-2 at days 1 to 5 after infection. (**F**) Left: Representative contour plots showing cytokine production by siLP T_H cells ($CD45^+CD90.2^+TCR\beta^+CD4^+Foxp3^-$). Right: Total IL-17A$^+$ and IL-17$^+$IL-22$^+$ siLP T_H cells. (**G**) Timed-pregnant *Rag1*^{KO} dams were intravenously injected with PBS or 10 μg of IL-6, and their offspring at 5 to 6 weeks of age (mCtr or mIL-6) were intraperitoneally injected with sorted 4×10^5 naïve T cells ($CD4^+CD45RB^{hi}CD25^-$) from wild-type donors. (**H** and **I**) Intestinal inflammation was assessed at 6 to 8 weeks after transfer by fecal lipocalin-2 (H) and total neutrophil numbers (I) in liLP. (**J**) Left: Representative contour plots of cytokine production by donor CD4$^+$ T cells in liLP after restimulation. Right: Total CD4$^+$ T cell numbers of IFN-γ, IL-17A, and double producers present in the liLP. In (B) and (C), the CFU detection limit was 10^2 CFU per gram of organ. Numbers in representative flow plots indicate mean ± SD. Data are representative of two or three independent experiments with one or two pregnant dams per group using three to six offspring per pregnancy. Each dot represents an individual mouse. *P < 0.05; **P < 0.01; ns, not significant [two-tailed unpaired Student's t test in (B), (C), (E), (F), and (H) to (J) and a log-rank test in (D)]. See also figs. S8 and S9.

of mucosal inflammation (52), was also significantly reduced in the offspring of IL-6–injected dams compared with controls (Fig. 6E). Further, antimicrobial peptides, such as *Reg3b* and *Pigr*, were significantly increased in IEC of offspring delivered by IL-6–injected dams at 2 days after infection (fig. S8A). Although the direct role of IL-17A in controlling *S.* Typhimurium remains unclear (53), infection with this bacterium has been associated with early type 3 immune responses (54). At day 5 after infection, the number and frequency of IL-17A- and IL-17A/IL-22–producing $CD4^+$ T cells, but not of ILCs, were significantly increased in the siLP of offspring of IL-6–injected dams compared with control dams (Fig. 6F and fig. S8B). Protection afforded by IL-6 injection in dams was significantly reduced in mice for which *Il6ra* was specifically deleted from IECs (fig. S8, C to E). Furthermore, offspring delivered by *yopM*-infected dams also displayed enhanced control of *S.* Typhimurium infection in a manner comparable to what was observed after IL-6 injection (fig. S8, F to H). Thus, both maternal infection and enhanced IL-6 signaling experienced by the fetus during pregnancy can promote antimicrobial defense through its direct impact on epithelial cells. No differences were observed in the ability of offspring delivered by IL-6–injected dams to control cutaneous infection with *Candida albicans*, which further supports the concept that, in this context, maternal imprinting of offspring is restricted to the gut compartment (fig. S9, A to C).

Heightened immunity can also come at the cost of increased susceptibility to inflammatory disorders. To test the possibility that maternal infection and/or IL-6 could contextually promote inflammatory responses in the offspring, we used two well-defined models of experimental colitis (55, 56). Using a naïve T cell transfer model, we found that offspring of IL-6–injected dams displayed enhanced intestinal inflammation compared with control offspring, as evidenced by increased fecal lipocalin and a higher number of neutrophils in the liLP (Fig. 6, G to I). Additionally, the number of transferred T cells producing IFN-γ, IL-17A, or both (IFN-γ^+ IL-$17A^+$) were significantly increased in the liLP of offspring from IL-6–injected dams compared with control offspring (Fig. 6J). The significant increase in double producers is of particular interest because this specific coexpression of cytokines is one of the characteristics of pathogenic T_H17 cells (57). Additionally, offspring of *yopM*-infected or IL-6–injected dams displayed enhanced pathology to dextran sulfate sodium (DSS)–induced colitis compared with controls, as evidenced by increased bodyweight loss and colon shortening (fig. S9, D to F). Thus, heightened intestinal immunity caused by maternal infection may also come at a cost of enhanced predisposition to inflammatory disorders.

Discussion

Optimal responses to microbial challenges are of utmost importance for host survival. Here, we showed that pregnancy represents a critical stage for tissue-specific immune education of the offspring. We demonstrated that direct responses of fetal epithelial cells to cytokines produced during maternal infections confer an enduring epigenetic memory to gut stem cells, a phenomenon that we propose contributes to both enhanced immunity and predisposition to inflammatory disorders. Recent studies have uncovered that, in adults, epithelial stem cells can develop memory of inflammatory insults, a phenomenon associated with accelerated responses to subsequent injuries (2, 3, 58). Our present work proposes that even a transient, mild infection encountered during prenatal development can impose lasting alterations to gut epithelial stem cells before birth, resulting in an altered tissue threshold of activation.

The impact of maternal infection was tissue specific and dominantly mediated by a single cytokine, IL-6. This observation raises an intriguing possibility that during fetal development, stem cells residing in different compartments may be educated by highly specific signals to develop optimal tissue immunity. Our findings also support the idea that infections experienced by the mother during pregnancy may optimize responses to immediate microbial threats in the offspring by augmenting responses at the target infectious sites. Further, IL-6 has previously been reported to be increased throughout pregnancy (59), a phenomenon that may broadly contribute to the education of the mammalian gut immune system.

Although our data indicate that maternal microbial exposure can be coopted by the fetus to develop optimal immune fitness, this phenomenon may also help to explain the marked increase in inflammatory disorders observed in the human population. Indeed, the altered maternal environment, together with the removal of regulatory microbial partners such as worms, may have contributed to shifting the outcome of maternal-induced immune maturation from protective to inflammatory. Further exploration of the maternal-fetal dialog in the face of microbial or environmental challenges may provide additional insights into our understanding of homeostatic and protective tissue immunity, as well as host predispositions to inflammatory diseases.

Materials and Methods

Mice

Specific pathogen–free (SPF) C57BL/6, *Lgr5*$^{EGFP\text{-}IRES\text{-}creERT2}$ (B6.129P2-*Lgr5*$^{tm1(cre/ERT2)/Cle}$/J, Jax008875), *Il6ra*$^{fl/fl}$ (B6.SJL-*Il6ra*$^{tm1.1Drew}$/J, Jax012944), and *Vil1*^{cre} (B6.Cg-Tg(Vil1-cre)1000Gum/J, Jax021504) mice were purchased from The Jackson Laboratory and Taconic Biosciences (SFB-negative barrier). Germ-free C57BL/6 mice were bred and maintained in the National Institute of Allergy and Infectious Diseases (NIAID) Microbiome Program gnotobiotic animal facility. CBir1 Tg mice were generated by Dr. C. Elson (University of Alabama, Birmingham), obtained under a material transfer agreement, and back-crossed to CD45.1-expressing mice (22). All mice were bred and maintained at an American Association for the Accreditation of Laboratory Animal Care (AAALAC)–accredited animal facility at NIAID and housed in accordance with procedures outlined in the *Guide for the Care and Use of Laboratory Animals*. All experiments were performed at NIAID under an animal study proposal (LISB19E and LHIM2E) approved by the NIAID Animal Care and Use Committee. For timed-pregnant breeding, males were first singly housed for 3 days and then cohoused with females for breeding. Males were separated from the breeding cage once a plug was observed. Littermate dams were used in each experiment to help normalize for differences in the microbiota. Offspring were weaned at 3 weeks after birth. Age-matched mice 5 to 8 weeks old from both sexes were used in each experiment unless specified otherwise.

Yersinia pseudotuberculosis infection

The *yopM* mutant strain of *Y. pseudotuberculosis* 32777 was grown overnight in 2× YT medium (Sigma-Aldrich) at 25°C with shaking at 200 rpm. Overnight cultures were centrifuged at 3000*g*, resuspended in phosphate-buffered saline (PBS), and adjusted to a density [absorbance at 600 nm (A_{600})] of 0.1 in PBS. Mice fasted overnight (12 to 16 hours) in new cages were orally administered 200 μl of *yopM* suspension [~2×10^7 colony-forming units (CFUs)]. To determine bacterial burden in the maternal spleen, liver, placenta, and fetal liver after *yopM* infection, tissues were homogenized through 70-μm filters with PBS. Tissue homogenates were serially diluted and plated onto MacConkey plates, and colonies were counted after incubation at 25°C for 48 hours. To measure bacterial burden in feces and fetal intestines, fecal DNA was extracted using phenol-chloroform, and intestinal DNA was extracted using TRIzol Reagent (Invitrogen). The *yscF* gene was quantified against a standard curve by quantitative PCR (forward primer 5′-ATGAGTAACTTCTCTG-GATTTACG-3′, reverse primer 5′-TTATGG-GAACTTCTGTAGGATG-3′).

Salmonella Typhimurium infection

A nalidixic acid-resistant strain of *S.* Typhimurium, IR715 (provided by Prof. A. Bäumler, University of California, Davis) was cultured in LB at 37°C with shaking at 200 rpm. Overnight cultures were centrifuged at 3000*g*, resuspended in PBS, and adjusted to an A_{600} of 0.001. Mice were fasted overnight (12 to 16 hours) before oral administration of 200 microliters of *S.* Typhimurium

suspension (~2×10^5 CFUs). Fecal samples were collected into preweighed tubes, homogenized in 500 μl of PBS with pipette tips, and vortexed for 5 s. At day 5 after infection, collected tissues were homogenized through 70-μm filters with PBS. The top fraction of fecal and tissues homogenates was serially diluted in PBS, spotted with a multichannel pipette onto LB agar with 50 mg/ml nalidixic acid, and incubated overnight at 37°C before counting CFUs. Remaining fecal homogenates were centrifuged at 3000*g* and stored at −80°C for lipocalin-2 measurement.

Adoptive transfer of CBir1 Tg CD4⁺ T cells

Cells from the spleen and the lymph nodes of CD45.1 CBir1 Tg mice were isolated by being passed through 70-μm filters. To enrich for $CD4^+$ T cells, single-cell suspensions were incubated with biotin-conjugated anti-CD8, anti-NK1.1, anti-CD11b, and anti-CD19 antibodies followed by anti-biotin microbeads (Miltenyi Biotec) and negatively selected by magnetic cell separation with MACS technology (Miltenyi Biotec). Then, 0.5 to 1.0 × 10^6 enriched $CD4^+$ T cells from CBir1 Tg mice were intravenously transferred by retroorbital injection to offspring delivered by control or transiently infected dams on a congenic CD45.2 background. Recipient mice were sacrificed at day 10 to 12 after transfer to assess donor cells in the siLP.

Cross-fostering experiments

Within 24 hours after birth, whole litters were removed from the original mother and gently mixed with new bedding in clean cages. Foster mothers were held to urinate on the pups. The cages were covered to avoid disturbances and monitored for at least 48 hours. Pups were nurtured by foster mothers until weaning at 3 weeks after birth.

Serum transfer experiments

Whole blood was collected from *yopM*-infected timed-pregnant dams at days 3 and 5 after infection. Blood samples were incubated at room temperature for 30 min and centrifuged at 2000*g* for 10 min. Sera were collected and transferred immediately by retroorbital injection to naïve timed-pregnant dams at gestation days 13.5 and 15.5. Each recipient received 200 μl of sera, combined from at least two mice, at each time point. Fifty microliters of serum collected from each mouse was plated onto MacConkey plates to assess CFUs.

In vivo cytokine stimulation and blockade

Timed-pregnant mice were intravenously injected with up to 10 μg of recombinant mouse cytokines (BioLegend) at gestation day 13.5. For IL-6 blockade experiments, timed-pregnant dams at gestation day 10.5 were injected intraperitoneally with either 1 mg of anti–IL-6 (MP5-20F3, BioXCell) or the IgG1 isotype control (HPRN, BioXCell) 1 hour before *yopM* infection.

Germ-free mice conventionalization

Offspring delivered by PBS or IL-6–injected germ-free timed-pregnant mice were kept in germ-free isolators and fostered by the same mothers until weaning. Subsequently, half of the litter was kept in isolators, whereas the other half was transferred using aseptic technique to a SPF facility at 3 weeks of age and analyzed at 5 to 8 weeks of age.

DSS-induced colitis

Offspring delivered by PBS-injected, *yopM*-infected, or IL-6–injected dams were provided drinking water with 2.5% DSS (ThermoFisher Scientific) for 7 days and allowed to recover for an additional 7 days. Fresh DSS was provided every 2 days. Body weights were monitored daily, and mice were sacrificed at day 14 after treatment.

Naïve CD4⁺ T cell transfer–induced colitis

$Rag1^{KO}$ females were bred with $Rag1^{KO}$ males. At day E13.5, timed-pregnant dams were injected with PBS or 10 μg of IL-6. Offspring delivered by PBS or IL-6–injected dams were intraperitoneally injected with 4 × 10^5 $CD4^+CD25^-CD45RB^{hi}$ T cells sorted from naïve mice. Mice were sacrificed at weeks 6 to 8 after transfer.

Cutaneous C. albicans infection

From a freezer stock, *C. albicans* (strain SC5314) was streaked onto a yeast extract peptone dextrose (YPD) agar plate and incubated at 37°C for 2 days. A single colony was cultured in YPD broth containing penicillin-streptomycin for 16 to 24 hours at 30°C. After two serial passages, *C. albicans* was centrifuged at 400*g* for 5 min, washed twice with sterile PBS, and reconstituted in PBS at 2 × 10^{10} cells/ml for infection. Mice were first anesthetized with a mixture of ketamine and xylazine (100 and 10 mg/kg of body weight, respectively). The stratum corneum was removed using a Dremel rotary tool for 10 s, and 10 μl of PBS or *C. albicans* was applied to the skin. Mice were sacrificed on days 2 and 5 after infection. Whole ears were removed, weighed, and homogenized in sterile medium before plating on BBL CHROMagar Candida Medium (BD Biosciences).

Milk collection

Dams at day 10 after parturition were separated from pups for 2 hours and anesthetized with a mixture of ketamine and xylazine (100 and 10 mg/kg of body weight). Dams were then intraperitoneally injected with 2 IU of oxytocin (Sigma-Aldrich). Milk was collected from mammary glands using a P10 pipette and stored at −80°C for subsequent analysis.

Tissue processing

Mice were euthanized with CO_2, perfused through the left ventricle of the heart with 10 ml of PBS, and the siLP, liLP, lung, and skin were collected and placed into cold complete medium (RPMI 1640 supplemented with 2 mM L-glutamine, 1 mM sodium pyruvate, 1 mM nonessential amino acids, 20 mM HEPES, 50 mM β-mercaptoethanol, 100 U/ml penicillin, and 100 mg/ml streptomycin). For siLP and liLP preparation, the Peyer's patches and the mesenteric adipose tissue were removed. Tissues were opened, washed in cold PBS to remove feces, cut into 1- to 2-cm segments, and treated with complete medium containing 5 mM EDTA and 0.145 mg/ml dithiothreitol for 20 min at 37°C with constant stirring. Tissues were shaken vigorously for 1 min and further digested with 10 ml of medium containing 500 mg/ml DNase I (Sigma-Aldrich) and 100 mg/ml Liberase TL (Roche) with continuous stirring at 37°C. Lungs were diced and incubated in 2 ml of prewarmed medium containing 500 mg/ml DNase I and 100 mg/ml Liberase TL for 25 min at 37°C. To isolate cells from the skin, ear pinnae were excised and separated into ventral and dorsal sheets, digested by placing the dermal side down in medium containing 500 mg/ml DNase I with 250 mg/ml Liberase TL, and incubated for 90 min at 37°C. Digested intestines, lung, and skin were passed through 70-μm cell strainers. Leukocytes were enriched by resuspension in 4 ml of 37.5% Percoll and centrifuged at 400*g* for 5 min. Cells were then washed with PBS before downstream analysis.

In vitro restimulation

To assess cytokine production potential, single-cell suspensions were restimulated in complete medium containing 10% fetal bovine serum, 50 ng/ml phorbol myristate acetate (Sigma-Aldrich), 5 mg/ml ionomycin (Sigma-Aldrich), and a 1:1000 dilution of GolgiPlug (BD Biosciences) for 2.5 hours at 37°C.

Flow cytometry analysis

The fluorophore-conjugated antibodies used are listed in table S1. For intracellular cytokine and transcription factor staining, after surface staining, cells were fixed and permeabilized using the Foxp3/Transcription Factor Staining Buffer Set (ThermoFisher Scientific) for at least 1 hour at 4°C and stained with fluorophore-conjugated antibodies for at least 1 hour at 4°C. All staining was performed in the presence of purified anti-mouse CD16/32 and purified rat gamma globulin. Dead cells were excluded using 4′,6-diamidino-2-phenylindol (DAPI, Sigma-Aldrich) or LIVE/DEAD Fixable Blue Dead Cell Stain Kit (Invitrogen Life Technologies). For phospho-STAT3 staining, after surface staining, cells were fixed with 4% paraformaldehyde at room temperature for 10 min and permeabilized

in prechilled methanol at −80°C for 1 hour. Cells were subsequently washed with PBS containing 0.5% Triton X-100 and 0.1% bovine serum albumin (BSA) and stained with a phycoerythrin-conjugated phospho-STAT3 antibody (Cell Signaling Technology) or the isotype control in the same buffer at 4°C. Cells were washed and analyzed immediately. Integrated mean fluorescence intensity reflects the total functional responses of a population determined by level of expression and frequency of positive cells (*60*).

16S rRNA gene profiling

Fecal DNA was extracted using the MagAttract PowerMicrobiome DNA/RNA kit (Qiagen). *16S* sequencing libraries were generated using 100 ng of purified DNA as template and the V4 region-targeting primers 515F (5′-GTGCCAGCMGCCGCGGTAA-3′) and 806R (5′-GGACTACHVGGGTWTCTAAT-3′). Amplicons were quantified, pooled at equimolar concentrations, and sequenced on a MiSeq (Illumina) using the v3 MiSeq Reagent Kit (Illumina). QIIME 2 was used to analyze *16S* data as previously described (*27*, *61*).

Confocal microscopy

Fetal intestines were isolated using a dissecting microscope. Adult small intestines were flushed with cold PBS and prepared using the Swiss-roll technique. Samples were incubated overnight in fixation and permeabilization buffer (BD Biosciences), followed by dehydration in 30% sucrose before embedding in OCT compound (Sakura Finetek). Then, 20-μm sections were cut on a CM3050S cryostat (Leica) and adhered to Superfrost Plus slides (VWR). Frozen sections were treated with prechilled acetone for 30 min at −80°C and subsequently permeabilized and blocked in PBS containing 0.3% Triton X-100 and 1% BSA (Sigma-Aldrich). Samples were stained with anti-IL6RA (BD Biosciences) and anti-EpCAM (BioLegend) at 37°C for 30 min. For fluorescence in situ hybridization, colons were fixed in Methacarn solution at 4°C overnight, washed in 70% ethanol, and embedded in paraffin. Longitudinal sections (5 to 25 μm) were hybridized to a bacterial *16S* rRNA gene probe: [AminoC6+Alexa488] – GCTGCCTCCCGTAGGACT – [AmC7-Q+Alexa488] (Eurofins MWG Operon) and counterstained with DAPI. Images were captured on a Leica TCS SP8 confocal microscope equipped with HyD and PMT detectors and a 40× oil objective (HC PL APO 40×/1.3 oil). Images were analyzed using Imaris (Bitplane).

IEC isolation and sorting

Freshly isolated and longitudinally opened samples were washed twice with gut wash buffer [Hanks' balanced salt solution supplemented with 2 mM L-glutamine, 1 mM sodium pyruvate, 1 mM nonessential amino acids, 20 mM HEPES, 100 U/ml penicillin, 100 mg/ml streptomycin, and 2% fetal calf serum (FCS)]. Tissues were cut into 1- to 2-cm segments and incubated with gut wash buffer containing 2 mM dithiothreitol in a 37°C water bath for 10 min. Tissues were vigorously shaken and subsequently incubated with fresh gut wash buffer containing 5 mM EDTA in a 37°C water bath for 7 min. EDTA-containing fractions were collected, and tissues were incubated with fresh EDTA for another 7 min. The two EDTA-containing fractions (enriched with crypts) were passed through 100-μm filters and centrifuged at 300*g* for 5 min. Cell pellets were digested with Dulbecco's modified Eagle's medium (DMEM) supplemented with 0.1 U/ml dispase (Life Technology) and 100 mg/ml DNase I for 8 min in a 37°C water bath. Digestion was neutralized with 2.5% FCS-DMEM, and the pellets were washed twice with gut wash buffer. Cell pellets were stained with antibodies against EpCAM, lineage (TCRβ, TCRγδ, CD8, and CD11b), CD31, and DAPI on ice for 30 min. For scRNA-seq, TotalSeq-A hashtag oligonucleotides (BioLegend) were included along with surface antibodies. IECs were sorted as the $DAPI^-CD31^-Lineage^-EpCAM^+$ population using a MA900 cell sorter (Sony) with a 100-μm chip.

Whole-tissue RNA-seq

Three centimeters of ileum was collected and extensively washed with PBS to remove feces. Samples were homogenized by bead-beating in tubes containing 2.8-mm beads and TRIzol reagent (ThermoFisher Scientific). RNA was extracted according to the TRIzol protocol. cDNA was synthesized with the Ultralow V4 kit (Clonetech), and sequencing libraries were subsequently prepared with the Nextera XT DNA prep kit (Illumina). RNA-seq reads were mapped with STAR to the mouse reference genome (mm10) with default parameters. Gene expression was measured with HOMER using analyzeRepeats.pl with parameters -condenseGenes and -tpm (for scatter plots) or -noadj (for differential gene expression analysis). Differential gene expression was assessed with HOMER's getDiffExpression.pl using DESeq2. Genes with a greater than a twofold change and a false discovery rate (FDR) smaller than 0.05 were considered differentially expressed.

FAST-ATAC-seq

Fast-ATAC-seq was performed according to a published protocol (*62*). Briefly, 10,000 fetal IECs ($EpCAM^+$) or adult EpSCs ($EpCAM^+Lgr5^+$) were sorted and pelleted by centrifugation at 500*g* for 5 min at 4°C. Supernatant was removed, and cell pellets were resuspended in 45 μl of transposase mixture (25 μl of Tagment DNA buffer, 2.5 μl of Tagment DNA enzyme, 0.5 μl of 1% digitonin, and 17 μl of H_2O) and incubated for 30 min at 37°C with agitation at 300 rpm. Tagmented DNA was purified using the QIAGEN MinElute Reaction Cleanup Kit, and purified DNA was eluted in 10 μl of elution buffer. Tagmented fragments were amplified with 10 to 15 PCR cycles on the basis of an amplification curve. After purification using the QIAGEN PCR cleanup kit, samples were sequenced single end on a NextSeq 550 (Illumina). ATAC-seq reads from three biological replicates were demultiplexed using bcl2fastq and mapped to the mouse reference genome (mm10) with STAR and default parameters. All biological replicates were run through the irreproducible discovery rate (IDR) framework, and only replicates that passed all filters (peak consistency between true replicates, peak consistency between pooled pseudoreplicates, and self-consistency for each replicate) and had an IDR threshold lower than 0.05 were kept. For final analysis, all peaks that passed IDR filter and were found in all replicates were used. In total, there were 24,938 peaks in adult EpSC cells from mCtr samples and 30,614 peaks in adult EpSC cells from mIL-6 samples. For analysis of fetal IECs, 49,787 peaks were found in mCtr samples and 43,813 in mIL-6 samples. For the IDR pipeline, open regions of chromatin were called using HOMER's findPeaks (with parameters -style factor, -center, -F 0, -L 0, -C 0, -fdr 0.01, -minDist 200, and -size 200) (*63*).

scRNA-seq and transcriptome analysis

$EpCAM^+$ IECs or $CD4^+$ T cells (2.5×10^4) were isolated from each sample using a Sony MA900 cell sorter. All samples were labeled with TotalSeqA hashtags antibodies (BioLegend), pooled, and encapsulated into droplets using a Chromium Single Cell Controller (10X Genomics), and libraries were prepared using Chromium Single Cell 3 Reagent Kits v3 (10X Genomics). The Controller was loaded with 2.5×10^4 cells per lane. mRNA was prepared following the 10X Genomics user guide, and the HTO library was prepared according to published guidelines (*64*). Libraries were sequenced on a NextSeq 550, with 10% of the lane occupied by the HTO library and 90% by the mRNA library. HTO was assigned to each single cell. Data were normalized, and lanes were combined using the scTransform function in Seurat. Data are displayed as uniform manifold approximation and projection (UMAP) using 25 dimensions. Intestinal cell subsets from each cluster were defined by the top 25 differentially expressed genes and identified on the basis of published datasets (*48*). Gene expression within each cluster was compared between offspring delivered by control or IL-6–exposed dams using Seurat.

RNA extraction, cDNA synthesis, and qPCR of sorted IECs

A total of 2×10^5 sorted IECs was lysed in RLT buffer, and total RNA was isolated using the

RNeasy Micro Kit (QIAGEN) according to the manufacturer's instructions. Total RNA was reverse-transcribed into cDNA using Omiscript RT Kit (QIAGEN) according to the manufacturer's instructions. qPCR was performed using TaqMan Gene Expression Assays on a Quantstudio 6 Flex Real-Time PCR System (Life Technologies). The housekeeping gene *Gapdh* was used to normalize critical threshold (CT) values. TaqMan primers are commercially available: *Gapdh* (Mm99999915_g1), *Reg3b* (Mm00440616_g1), *Reg3g* (Mm0044127_m1), *Pigr* (Mm01288210_g1), and *Dmbt1* (Mm00455996_m1). Analysis was conducted using the ΔCT method.

Three-chamber social behavior tests

Eight-week-old offspring were tested for sociability using three-chamber social tests. Mice were habituated in the center chamber for 10 min, followed by a 10-min habituation session with access to all three empty chambers. After the two habituation sessions, the 10-min sociability test was conducted. An inverted wire pencil cup (novel object) was placed in one of the side chambers and the other side chamber had an inverted wire pencil cup containing an age- and sexed-matched C57BL6 mouse (novel mouse). Frequency to enter and time in each chamber was analyzed using Noldus Ethovision software (Noldus Information Tech Inc. Leesburg, VA, USA).

Measurement of cytokines and chemokines

Sera cytokine and chemokine levels were quantified using the Cytokine & Chemokine Convenience 36-Plex Mouse ProcartaPlex Panel 1A (Invitrogen) according to the manufacturer's instructions.

Measurement of serum amyloid A

Three-centimeter intestinal segments from the duodenum, jejunum, and ileum were collected and extensively washed with PBS to remove feces. Samples were homogenized by bead-beating with 400 μl of RIPA lysis buffer (Chem Cruz) containing proteinase inhibitor in tubes containing 2.8-mm beads. Extracted samples were centrifuged at 10,000*g* for 10 min at 4°C to remove debris. Serum amyloid A levels were quantified using the Mouse Serum Amyloid A Quantikine ELISA Kit (R&D) according to the manufacturer's instructions.

Measurement of lipocalin-2

Lipocalin-2 levels in fecal samples were measured using the Mouse Lipocalin-2/NGAL Quantikine ELISA Kit (R&D Systems) according to the manufacturer's instructions.

Measurement of IL-6

IL-6 levels in serum and breast milk were measured using the Mouse IL-6 Quantikine ELISA Kit (R&D Systems) according to the manufacturer's instructions.

Statistical analysis

Groups were compared with Prism software (GraphPad).

REFERENCES AND NOTES

1. M. G. Netea *et al*., Defining trained immunity and its role in health and disease. *Nat. Rev. Immunol.* **20**, 375–388 (2020). doi: 10.1038/s41577-020-0285-6; pmid: 32132681
2. S. Naik *et al*., Inflammatory memory sensitizes skin epithelial stem cells to tissue damage. *Nature* **550**, 475–480 (2017). doi: 10.1038/nature24271; pmid: 29045388
3. J. Ordovas-Montanes *et al*., Allergic inflammatory memory in human respiratory epithelial progenitor cells. *Nature* **560**, 649–654 (2018). doi: 10.1038/s41586-018-0449-8; pmid: 30135581
4. R. S. Moore, R. Kaletsky, C. T. Murphy, Piwi/PRG-1 argonaute and TGF-β mediate transgenerational learned pathogenic avoidance. *Cell* **177**, 1827–1841.e12 (2019). doi: 10.1016/j.cell.2019.05.024; pmid: 31178117
5. G. Tetreau, J. Dhinaut, B. Gourbal, Y. Moret, Trans-generational immune priming in invertebrates: Current knowledge and future prospects. *Front. Immunol.* **10**, 1938 (2019). doi: 10.3389/fimmu.2019.01938; pmid: 31475001
6. M. L. T. Berendsen *et al*., Maternal priming: Bacillus Calmette-Guérin (BCG) vaccine scarring in mothers enhances the survival of their child with a BCG vaccine scar. *J. Pediatric Infect. Dis. Soc.* **9**, 166–172 (2020). doi: 10.1093/jpids/piy142; pmid: 30715451
7. B. de Laval *et al*., C/EBPβ-dependent epigenetic memory induces trained immunity in hematopoietic stem cells. *Cell Stem Cell* **26**, 657–674.e8 (2020). doi: 10.1016/j.stem.2020.01.017; pmid: 32169166
8. S. P. Rosshart *et al*., Wild mouse gut microbiota promotes host fitness and improves disease resistance. *Cell* **171**, 1015–1028.e13 (2017). doi: 10.1016/j.cell.2017.09.016; pmid: 29056339
9. L. K. Beura *et al*., Normalizing the environment recapitulates adult human immune traits in laboratory mice. *Nature* **532**, 512–516 (2016). doi: 10.1038/nature17655; pmid: 27096360
10. G. Mor, P. Aldo, A. B. Alvero, The unique immunological and microbial aspects of pregnancy. *Nat. Rev. Immunol.* **17**, 469–482 (2017). doi: 10.1038/nri.2017.64; pmid: 28627518
11. S. Niewiesk, Maternal antibodies: Clinical significance, mechanism of interference with immune responses, and possible vaccination strategies. *Front. Immunol.* **5**, 446 (2014). doi: 10.3389/fimmu.2014.00446; pmid: 25278941
12. G. Caballero-Flores *et al*., Maternal immunization confers protection to the offspring against an attaching and effacing pathogen through delivery of IgG in breast milk. *Cell Host Microbe* **25**, 313–323.e4 (2019). doi: 10.1016/j.chom.2018.12.015; pmid: 30686564
13. M. G. Darby *et al*., Pre-conception maternal helminth infection transfers via nursing long-lasting cellular immunity against helminths to offspring. *Sci. Adv.* **5**, eaav3058 (2019). doi: 10.1126/sciadv.aav3058; pmid: 31236458
14. E. Y. Hsiao, S. W. McBride, J. Chow, S. K. Mazmanian, P. H. Patterson, Modeling an autism risk factor in mice leads to permanent immune dysregulation. *Proc. Natl. Acad. Sci. U.S.A.* **109**, 12776–12781 (2012). doi: 10.1073/pnas.1202556109; pmid: 22802640
15. R. L. Goldenberg, J. C. Hauth, W. W. Andrews, Intrauterine infection and preterm delivery. *N. Engl. J. Med.* **342**, 1500–1507 (2000). doi: 10.1056/NEJM200005183422007; pmid: 10816189
16. R. Medzhitov, D. S. Schneider, M. P. Soares, Disease tolerance as a defense strategy. *Science* **335**, 936–941 (2012). doi: 10.1126/science.1214935; pmid: 22363001
17. J. L. McCarville, J. S. Ayres, Disease tolerance: Concept and mechanisms. *Curr. Opin. Immunol.* **50**, 88–93 (2018). doi: 10.1016/j.coi.2017.12.003; pmid: 29253642
18. S. J. Han *et al*., White adipose tissue is a reservoir for memory T cells and promotes protective memory responses to infection. *Immunity* **47**, 1154–1168.e6 (2017). doi: 10.1016/j.immuni.2017.11.009; pmid: 29221731
19. M. W. McCoy, M. L. Marré, C. F. Lesser, J. Mecsas, The C-terminal tail of *Yersinia pseudotuberculosis* YopM is critical for interacting with RSK1 and for virulence. *Infect. Immun.* **78**, 2584–2598 (2010). doi: 10.1128/IAI.00141-10; pmid: 20368345
20. K. Miyawaki *et al*., CD41 marks the initial myelo-erythroid lineage specification in adult mouse hematopoiesis: Redefinition of murine common myeloid progenitor. *Stem Cells* **33**, 976–987 (2015). doi: 10.1002/stem.1906; pmid: 25446279
21. K. E. McGrath *et al*., Distinct sources of hematopoietic progenitors emerge before HSCs and provide functional blood cells in the mammalian embryo. *Cell Rep.* **11**, 1892–1904 (2015). doi: 10.1016/j.celrep.2015.05.036; pmid: 26095363
22. Y. Cong, T. Feng, K. Fujihashi, T. R. Schoeb, C. O. Elson, A dominant, coordinated T regulatory cell-IgA response to the intestinal microbiota. *Proc. Natl. Acad. Sci. U.S.A.* **106**, 19256–19261 (2009). doi: 10.1073/pnas.0812681106; pmid: 19889972
23. T. W. Hand *et al*., Acute gastrointestinal infection induces long-lived microbiota-specific T cell responses. *Science* **337**, 1553–1556 (2012). doi: 10.1126/science.1220961; pmid: 22923434
24. T. Sano *et al*., An IL-23R/IL-22 circuit regulates epithelial serum amyloid A to promote local effector T_H17 responses. *Cell* **163**, 381–393 (2015). doi: 10.1016/j.cell.2015.08.061; pmid: 26411290
25. M. J. Molloy *et al*., Intraluminal containment of commensal outgrowth in the gut during infection-induced dysbiosis. *Cell Host Microbe* **14**, 318–328 (2013). doi: 10.1016/j.chom.2013.08.003; pmid: 24034617
26. V. J. Carrión *et al*., Pathogen-induced activation of disease-suppressive functions in the endophytic root microbiome. *Science* **366**, 606–612 (2019). doi: 10.1126/science.aaw9285; pmid: 31672892
27. A. Stacy *et al*., Infection trains the host for microbiota-enhanced resistance to pathogens. *Cell* **184**, 615–627.e17 (2021). doi: 10.1016/j.cell.2020.12.011; pmid: 33453153
28. M. V. Zaretsky, J. M. Alexander, W. Byrd, R. E. Bawdon, Transfer of inflammatory cytokines across the placenta. *Obstet. Gynecol.* **103**, 546–550 (2004). doi: 10.1097/01.AOG.0000114980.40445.83; pmid: 14990420
29. S. C. Ganal-Vonarburg, M. W. Hornef, A. J. Macpherson, Microbial-host molecular exchange and its functional consequences in early mammalian life. *Science* **368**, 604–607 (2020). doi: 10.1126/science.aba0478; pmid: 32381716
30. J. Hoge *et al*., IL-6 controls the innate immune response against Listeria monocytogenes via classical IL-6 signaling. *J. Immunol.* **190**, 703–711 (2013). doi: 10.4049/jimmunol.1201044; pmid: 23241882
31. S. M. Chen, C. P. Lin, J. D. Tsai, Y. H. Chao, J. N. Sheu, The significance of serum and fecal levels of interleukin-6 and interleukin-8 in hospitalized children with acute rotavirus and norovirus gastroenteritis. *Pediatr. Neonatol.* **55**, 120–126 (2014). doi: 10.1016/j.pedneo.2013.05.008; pmid: 23899552
32. G. B. Choi *et al*., The maternal interleukin-17a pathway in mice promotes autism-like phenotypes in offspring. *Science* **351**, 933–939 (2016). doi: 10.1126/science.aad0314; pmid: 26822608
33. J. R. Prins, N. Gomez-Lopez, S. A. Robertson, Interleukin-6 in pregnancy and gestational disorders. *J. Reprod. Immunol.* **95**, 1–14 (2012). doi: 10.1016/j.jri.2012.05.004; pmid: 22819759
34. S. Kim *et al*., Maternal gut bacteria promote neurodevelopmental abnormalities in mouse offspring. *Nature* **549**, 528–532 (2017). doi: 10.1038/nature23910; pmid: 28902840
35. Y. Lee *et al*., Induction and molecular signature of pathogenic TH17 cells. *Nat. Immunol.* **13**, 991–999 (2012). doi: 10.1038/ni.2416; pmid: 22961052
36. J. Y. Lee *et al*., Serum amyloid A proteins induce pathogenic T_H17 cells and promote inflammatory disease. *Cell* **180**, 79–91.e16 (2020). doi: 10.1016/j.cell.2019.11.026; pmid: 31866067
37. M. Murakami, D. Kamimura, T. Hirano, Pleiotropy and specificity: Insights from the interleukin 6 family of cytokines. *Immunity* **50**, 812–831 (2019). doi: 10.1016/j.immuni.2019.03.027; pmid: 30995501
38. J. Dahlgren, A. M. Samuelsson, T. Jansson, A. Holmäng, Interleukin-6 in the maternal circulation reaches the rat fetus in mid-gestation. *Pediatr. Res.* **60**, 147–151 (2006). doi: 10.1203/01.pdr.0000230026.74139.18; pmid: 16864694
39. L. Goetzl, T. Evans, J. Rivers, M. S. Suresh, E. Lieberman, Elevated maternal and fetal serum interleukin-6 levels are associated with epidural fever. *Am. J. Obstet. Gynecol.* **187**, 834–838 (2002). doi: 10.1067/mob.2002.127135; pmid: 12388959
40. D. Fawkner-Corbett *et al*., Spatiotemporal analysis of human intestinal development at single-cell resolution. *Cell* **184**, 810–826.e23 (2021). doi: 10.1016/j.cell.2020.12.016; pmid: 33406409

41. M. P. Verzi *et al*., Differentiation-specific histone modifications reveal dynamic chromatin interactions and partners for the intestinal transcription factor CDX2. *Dev. Cell* **19**, 713–726 (2010). doi: 10.1016/j.devcel.2010.10.006; pmid: 21074721
42. U. Jadhav *et al*., Dynamic reorganization of chromatin accessibility signatures during dedifferentiation of secretory precursors into Lgr5+ intestinal stem cells. *Cell Stem Cell* **21**, 65–77.e5 (2017). doi: 10.1016/j.stem.2017.05.001; pmid: 28648363
43. R. Francis *et al*., Gastrointestinal transcription factors drive lineage-specific developmental programs in organ specification and cancer. *Sci. Adv.* **5**, eaax8898 (2019). doi: 10.1126/sciadv.aax8898; pmid: 31844668
44. J. Guiu *et al*., Tracing the origin of adult intestinal stem cells. *Nature* **570**, 107–111 (2019). doi: 10.1038/s41586-019-1212-5; pmid: 31092921
45. A. M. Chin, D. R. Hill, M. Aurora, J. R. Spence, Morphogenesis and maturation of the embryonic and postnatal intestine. *Semin. Cell Dev. Biol.* **66**, 81–93 (2017). doi: 10.1016/j.semcdb.2017.01.011; pmid: 28161556
46. Z. Al Nabhani *et al*., A weaning reaction to microbiota is required for resistance to immunopathologies in the adult. *Immunity* **50**, 1276–1288.e5 (2019). doi: 10.1016/j.immuni.2019.02.014; pmid: 30902637
47. N. Barker *et al*., Identification of stem cells in small intestine and colon by marker gene Lgr5. *Nature* **449**, 1003–1007 (2007). doi: 10.1038/nature06196; pmid: 17934449
48. A. L. Haber *et al*., A single-cell survey of the small intestinal epithelium. *Nature* **551**, 333–339 (2017). doi: 10.1038/nature24489; pmid: 29144463
49. M. Biton *et al*., T helper cell cytokines modulate intestinal stem cell renewal and differentiation. *Cell* **175**, 1307–1320.e22 (2018). doi: 10.1016/j.cell.2018.10.008; pmid: 30392957
50. M. Koyama *et al*., MHC class II antigen presentation by the intestinal epithelium initiates graft-versus-host disease and is influenced by the microbiota. *Immunity* **51**, 885–898.e887 (2019). doi: 10.1016/j.immuni.2019.08.011; pmid: 31542340
51. E. M. Velazquez *et al*., Endogenous Enterobacteriaceae underlie variation in susceptibility to Salmonella infection. *Nat. Microbiol.* **4**, 1057–1064 (2019). doi: 10.1038/s41564-019-0407-8; pmid: 30911125
52. B. Chassaing *et al*., Fecal lipocalin 2, a sensitive and broadly dynamic non-invasive biomarker for intestinal inflammation. *PLOS ONE* **7**, e44328 (2012). doi: 10.1371/journal.pone.0044328; pmid: 22957064
53. M. J. McGeachy, S. J. McSorley, Microbial-induced T_H17: Superhero or supervillain? *J. Immunol.* **189**, 3285–3291 (2012). doi: 10.4049/jimmunol.1201834; pmid: 22997231
54. K. Geddes *et al*., Identification of an innate T helper type 17 response to intestinal bacterial pathogens. *Nat. Med.* **17**, 837–844 (2011). doi: 10.1038/nm.2391; pmid: 21666695
55. B. Chassaing, J. D. Aitken, M. Malleshappa, M. Vijay-Kumar, Dextran sulfate sodium (DSS)-induced colitis in mice. *Curr. Protoc. Immunol.* **104**, 15.25.1–15.25.14 (2014). doi: 10.1002/0471142735.im1525s104; pmid: 24510619
56. C. Asseman, S. Read, F. Powrie, Colitogenic Th1 cells are present in the antigen-experienced T cell pool in normal mice: Control by CD4+ regulatory T cells and IL-10. *J. Immunol.* **171**, 971–978 (2003). doi: 10.4049/jimmunol.171.2.971; pmid: 12847269
57. T. Krausgruber *et al*., T-bet is a key modulator of IL-23-driven pathogenic CD4(+) T cell responses in the intestine. *Nat. Commun.* **7**, 11627 (2016). doi: 10.1038/ncomms11627; pmid: 27193261
58. S. Beyaz *et al*., High-fat diet enhances stemness and tumorigenicity of intestinal progenitors. *Nature* **531**, 53–58 (2016). doi: 10.1038/nature17173; pmid: 26935695
59. L. M. Christian, K. Porter, Longitudinal changes in serum proinflammatory markers across pregnancy and postpartum: Effects of maternal body mass index. *Cytokine* **70**, 134–140 (2014). doi: 10.1016/j.cyto.2014.06.018; pmid: 25082648
60. P. Shooshtari *et al*., Correlation analysis of intracellular and secreted cytokines via the generalized integrated mean fluorescence intensity. *Cytometry A* **77**, 873–880 (2010). doi: 10.1002/cyto.a.20943; pmid: 20629196
61. E. Bolyen *et al*., Reproducible, interactive, scalable and extensible microbiome data science using QIIME 2. *Nat. Biotechnol.* **37**, 852–857 (2019). doi: 10.1038/s41587-019-0209-9; pmid: 31341288
62. M. R. Corces *et al*., Lineage-specific and single-cell chromatin accessibility charts human hematopoiesis and leukemia evolution. *Nat. Genet.* **48**, 1193–1203 (2016). doi: 10.1038/ng.3646; pmid: 27526324
63. V. M. Link *et al*., Analysis of genetically diverse macrophages reveals local and domain-wide mechanisms that control transcription factor binding and function. *Cell* **173**, 1796–1809.e17 (2018). doi: 10.1016/j.cell.2018.04.018; pmid: 29779944
64. M. Stoeckius *et al*., Cell Hashing with barcoded antibodies enables multiplexing and doublet detection for single cell genomics. *Genome Biol.* **19**, 224 (2018). doi: 10.1186/s13059-018-1603-1; pmid: 30567574

ACKNOWLEDGMENTS

We thank T. Hawley, J. Chen, S. Mistry, G. Koroleva, K. Beacht, E. Lewis, the NIAID animal facility, and the NIAID Microbiome Program gnotobiotic animal facility for technical support. We thank K. Mao, A. Gola, and the NIAID Biological Imaging Facility for providing support for confocal imaging. We thank all Belkaid laboratory members, especially S. Tamoutounour, P. Kulalert, M. Enamorado, and E. Ansaldo, for providing constructive feedback on this project and for critical reading of this manuscript. **Funding:** Y.B. is supported by the Division of Intramural Research of NIAID (grants ZIA-AI001115 and ZIA-AI001132). H.A.C. is supported by the Division of Intramural Research of the NIMH (grant ZIA-MH002784). M.S.L. is supported by the Division of Intramural Research of the NIAID (grant ZIA-AI001175). A.I.L. is supported by the Human Frontier Science Program (grant LT000191/2018). A.S. is supported by the National Institute of General Medical Sciences (NIGMS) Postdoctoral Research Associate (PRAT) fellowship program (grant 1FI2GM128736). **Author contributions**: A.I.L. and Y.B. designed the study experiments and wrote the manuscript. A.I.L. performed experiments and analyzed the data. T.M., T.K.F., and D.S.L.-J. participated in performing experiments. V.M.L. analyzed RNA-seq and ATAC-seq data. A.S provided expertise in *Salmonella* Typhimurium infection and analyzed 16*S* data. H.-Y.S. provided expertise in ATAC-seq. O.J.H. provided intellectual expertise. J.V.D. and M.S.L. provided expertise in *C. albicans* infection. R.-M.K. and H.A.C. performed and interpreted data from behavior studies. S.-J.H. provided intellectual expertise, participated in experiments, and helped to interpret experimental results. **Competing interests:** The authors declare no competing interests. **Data and materials availability:** 16*S* sequencing, ATAC-seq, RNA-seq, and scRNA-seq data were deposited into the NCBI Sequence Read Archive (accession numbers PRJNA666968, GSE158950, and GSE159149). All data are available in the main text or the supplementary materials.

SUPPLEMENTARY MATERIALS

science.sciencemag.org/content/373/6558/eabf3002/suppl/DC1
Figs. S1 to S9
Table S1
MDAR Reproducibility Checklist

View/request a protocol for this paper from *Bio-protocol*.

18 October 2020; accepted 7 July 2021
10.1126/science.abf3002

Prenatal maternal infection promotes tissue-specific immunity and inflammation in offspring

Ai Ing Lim, Taryn McFadden, Verena M. Link, Seong-Ji Han, Rose-Marie Karlsson, Apollo Stacy, Taylor K. Farley, Djalma S. Lima-Junior, Oliver J. Harrison, Jigar V. Desai, Michail S. Lionakis, Han-Yu Shih, Heather A. Cameron, and Yasmine Belkaid

Science **373** (6558), eabf3002. DOI: 10.1126/science.abf3002

Mom's IL-6 rewires baby's gut immunity

Most infections that occur during pregnancy are mild and transient. However, whether such pathogen encounters can shape the long-term trajectory of the offspring's immune system remains unclear. Lim *et al*. infected pregnant mice with the common food-borne pathogen *Yersinia pseudotuberculosis* (YopM) (see the Perspective by Amir and Zeng). Although the infection was maternally restricted and short-lived, the offspring harbored greater numbers of intestinal T helper 17 cells into adulthood. Interleukin-6 (IL-6) mediated this tissue-restricted effect by acting on fetal intestinal epithelium during development. Although offspring from mothers infected with YopM or injected with IL-6 showed enhanced resistance to oral infection with *Salmonella* Typhimurium, they also exhibited higher susceptibility toward enteric inflammatory disease. —STS